2012

HCN1 Immunoreactivity of α-motoneurons Following Peripheral Nerve Injury

Saif Ahmed
Wright State University

HCN1 immunoreactivity of α-motoneurons following peripheral nerve injury

A thesis submitted in partial fulfillment
of the requirements for the degree of
Master of Science

By

Saif Ahmed
B.S., The Ohio State University 2010

2012
Wright State University

WRIGHT STATE UNIVERSITY

GRADUATE SCHOOL

June 11, 2012

I HEREBY RECOMMEND THAT THE THESIS PREPARED UNDER MY SUPERVISION BY Saif Ahmed ENTITLED HCN1 Immunoreactivity of α-motoneurons following peripheral nerve injury BE ACCEPTED IN PARTIAL FULFILLMENT OF THE REQUIREMENTS FOR THE DEGREE OF Master of Science.

_____
Robert E.W. Fyffe, Ph.D.
Thesis Director

_____
Timothy C. Cope, Ph.D.
Department Chair

Committee on
Final Examination

_____
Robert E.W. Fyffe, Ph.D.

_____
Timothy C. Cope, Ph.D.

_____
Robert W. Putnam, Ph.D.

_____
Andrew Hsu, Ph.D.
Dean, Graduate School

ABSTRACT

Ahmed, Saif M.S., Department of Neuroscience, Cell Biology, and Physiology, Wright State University, 2012. HCN1 Immunoreactivity of α-motoneurons Following Peripheral Nerve Injury

Peripheral axotomy causes significant alterations in intrinsic motoneuron activity and excitability. Despite successful reinnervation of peripheral targets after injury, the recovery of motor function is incomplete. Following axotomy in the adult cat, there is an increase in the afterhyperpolarization (AHP) of the action potential in specific motoneuron types. AHP duration can be inversely correlated with the amount of I_h or sag current and further shaped through SK (Small conductance calcium-activated potassium) channel currents (Gustafsson & Pinter, 1985; Kuno, Miyata, & Muñoz-Martinez, 1974a). Hyperpolarizing-cyclic nucleotide gated (HCN) channels underlie sag currents and are critical to neuronal function by their unique property of a reverse voltage-dependence that leads to activation upon hyperpolarization. There are four isoforms of HCN channels, one of which, HCN1, is expressed in motoneurons. Because there is an increase in AHP after injury, we hypothesize that there will be a decrease in expression of HCN1 immunoreactivity (IR) in the medial and lateral gastrocnemius (MG/LG) α-motoneurons following tibial nerve axotomy. To test this hypothesis, we used immunohistochemical approaches in two in vivo injury models, namely the tibial nerve crush model, that

permits peripheral reinnervation of the peripheral targets and the tibial nerve ligation model, that prevents peripheral reinnervation from occurring, thus allowing us to distinguish between mechanisms and their dependency on proper reinnervation of peripheral targets. Lumbar spinal cord tissue was analyzed using immunohistochemical techniques to identify retrogradely labeled, injured MG/LG α-motoneurons and HCN1-IR. These data suggest that following injury there is a decrease in HCN1-IR followed by a peripheral reinnervation-dependent recovery.

Table of Contents

List of Tables and Figures

Acknowledgements

I would first like to thank my advisor, Dr. Robert E.W. Fyffe for granting me an opportunity in the lab and taking the time amidst a busy schedule to mentor, critique, and advise my project.

I also have to express by deep appreciation and gratitude to Shannon Romer, whom without, this project would not exist. All my knowledge and training of scientific technique, experimental design, scientific writing was possible through her insightful mentorship and constant support.

I would also like to thank Adam Deardorff, Jackie Sisco, Valerie Neff, Patrick Sonner, and Lan-Anh Bui. All of who have been critical to advising my progress, teaching me the use of equipment and software, and creating a exciting, scholarly, as well as fun workplace.

Finally, I would like to thank my parents Aijaz and Samina, my brother Nawaz, and my sister Sana. My family has always expressed support and genuine interest in my education and scientific work and for that I am grateful.

I. Introduction

More than 20 million Americans are afflicted by peripheral nerve injury. The ability for the peripheral nervous system to regenerate after injury has been studied extensively. However, despite this ability to regenerate, full functional recovery seldom occurs after reinnervation. This absence in recovery is described as a loss of motor control, touch, pain, temperature and/or sense of position in space. Peripheral nerve injury can occur after significant events of blunt trauma or penetrating wounds i.e. motor vehicle accidents and sports injuries, or via compression of the nerve in cases like carpel tunnel syndrome (Eser, Aktekin, Bodur, & Atan, 2009). Previous electrophysiological studies have given some insight into changes in intrinsic motoneuron properties, however, by using the latest imaging and immunohistochemical techniques, we can now visualize, describe, and analyze the specific changes in ion channels that underlie these electrophysiological findings. Currently, clinicians record nerve conduction velocities in order to diagnose patients with the symptoms of peripheral nerve injury listed above. Discussed in this thesis, are some of the intrinsic motoneuron properties that affect the conduction velocity and change with injury. Studies like this attempt to produce clinical advancements in the treatment and recovery for nerve injuries, as well as provide insight to neurodegenerative disorders that exhibit similar physiological properties.

II. Background:

A1. Spinal Cord: Anatomy

The nervous system is classified into two categories: the central nervous system (CNS) consisting of the brain and spinal cord, and the peripheral nervous system (PNS) consisting of nerves that connect the CNS to the limbs and organs as well as transmit sensory information to the CNS. As the focus of this study attempts to provide insight to changes in motor control, attention will be directed to the intrinsic properties of motoneurons (MNs). Spinal MNs have cell bodies that are located in the spinal cord and have axons that project out into the periphery to its specific target. Because our model utilized rat MNs that innervated the medial gastrocnemius and lateral gastrocnemius (MG/LG) muscles, MNs in the lumbar region of the spinal cord were analyzed (J. Swett, Wikholm, Blanks, & Swett, 1986). The gastrocnemius nerve is a branch of the tibial nerve, which stems from the sciatic nerve. MNs that innervate the MG/LG muscle are located in a rostro-caudal column from the middle of Lumbar 4 (L4) through the rostral Lumbar 6 (L6) regions of the spinal cord (J. Swett et al., 1986). Cytoarchitecturally, the rat lumbar spinal cord is organized in ten laminae. The ventral horn consists of lamina I through lamina VI, and the dorsal horn consists of lamina VII through lamina X (Molander, Xu, & Grant, 1984). In the lamina IX resides the MN pool which innervates the MG/LG muscles (Molander et al., 1984). Hence, this study focused on the cell bodies

and proximal dendrites of MNs, which are located in lamina IX portion of the dorsal horn in the L4, L5, and L6 regions of the spinal cord.

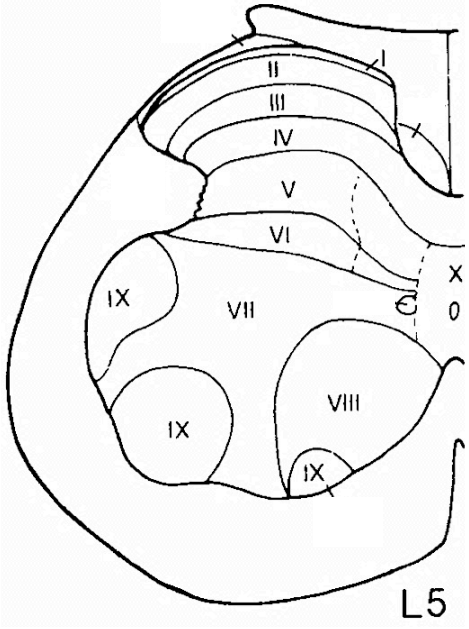

Figure A. Cross-section of the Lumbar 5 region of the spinal cord. Roman numerals indicate the spinal cord lamina (Molander, Xu, & Grant, 1984)

A2. Spinal Cord: Properties of the Action Potential

Information is carried through our nervous system via electrical and chemical signals between neurons. These signals create changes in the membrane potential of a neuron, which consequently create a current that travels within neurons. Contributions to the change in membrane potential and current are dictated by the chemical or electrical activation of various ion channels throughout neurons (*as reviewed in* E. R. Kandel, Schwartz, & Jessell, 1991). The release of neurotransmitters between axon terminals and neurons can initiate a phenomenon known as an "action potential" which is a rapid depolarization of membrane potential followed by repolarization then a hyperpolarization phase. These action potentials occur when a membrane potential reaches a "threshold" potential, causing the activation of a series of inward-rectifying ion channels (usually

sodium ions travelling through fast-opening, sodium-specific ion channels) followed by the deactivation of inward-rectifying ion channels and the activation of outwardly rectifying channels (usually slower potassium-specific ion channels). After repolarization, a refractory period known as the afterhyperpolarization (AHP) phase occurs. During this phase, the neuronal membrane potential falls below its resting membrane potential, and an action potential is less likely to be initiated. The duration of the AHP determines how quickly a successive action potential can occur and ultimately adjusts the firing rate. The speed and frequency of these action potentials modulates the communication throughout the nervous system and is dictated by the density, distribution, composition, expression and gating properties of ion channels. Hence, the study of membrane properties that affect the initiation, speed, and frequency of action potentials can provide detailed insight into the communication between neurons in the nervous system.

A3. Spinal Cord: Motoneurons

The soma, dendrites, axon, and presynaptic terminals are the four defining morphological regions on a neuron. The soma is the cell body of the neuron, which houses the metabolic organelles and activity. Extending from the neuron soma are several branched processes called dendrites, which receive inputs from other nerve cells, receptors, and glia. Action potentials generated from the neuron propagate down the long narrow tubular structure called the axon. The axon is covered in myelin sheath, a fatty insulation that increases the conductance and speed of electrical signals. Synaptic inputs from the dendrites converge and sum into a single action potential at the axon hillock, the

initial segment of the axon. Action potentials are regenerated at unmyelinated segments of the axon, termed the Nodes of Ranvier, possibly compensating for the unavoidable leak conductance across the axon despite its insulation.

Neurons located in the spinal cord are known as spinal MNs. 95% - 97% of the membrane surface area of MNs is located in the dendritic arbor (Fyffe, 2001; Lüscher & Clamann, 1992). The total membrane area of a cat hind limb alpha MN can range from 250,000 to 750,000 μm^2, while the soma only constitutes 6,000-15,000 μm^2 (Lüscher & Clamann, 1992). The dendritic arbor of cat alpha MNs in the lumbar spinal cord is radial and can extend up to 1600 μm from the soma in the rostro-caudal direction; extending into the ventral horn and reaching as dorsal as lamina V or VI (A. G. Brown & Fyffe, 1981; Fyffe, 2001; Lüscher & Clamann, 1992). Fully reconstructed hind limb MNs of the cat have 7-18 primary dendrites (A. G. Brown & Fyffe, 1981). In comparison with the cat, rat triceps surae MNs have smaller average surface areas (150,000μm^2 vs. 560,000μm^2), fewer primary dendrites (8 vs. 12), and shorter total dendritic lengths (36mm vs. 105mm). However, there is not a species difference in number of contacts on the dendritic arbor; therefore, hindlimb rat MNs have more contacts per unit of dendritic length (X. Y. Chen & Wolpaw, 1994). For all cat MNs, the mean diameter of the stem dendrite and the mean diameter of the cell body share a strong relationship (Lüscher & Clamann, 1992). In hindlimb cat MNs, the diameter of the stem dendrite is positively correlated with the dendritic membrane area, the combined dendritic length, and the number of terminations (Lüscher & Clamann, 1992). Similarly, in hindlimb rat MNs diameter of the stem dendrite is also positively correlated with combined dendritic length, surface area, and volume (X. Y. Chen & Wolpaw, 1994).

A4. Spinal Cord: Motor Unit

Two main types of somatic MNs (MNs that innervate skeletal muscle) exist. α-MNs originate in the ventral horn and have axons that project from the spinal cord through the ventral root and innervate 100-1000 extrafusal muscle fibers throughout the muscle. γ-MNs innervate intrafusal muscle located within the muscle spindle. Sensory fibers within the muscle spindle detect the amount of stretch and can adjust tension either through changes in intrafusal stretch or via Ia afferents that synapse onto the α-MNs depending on the appropriate feedback proprioception. In addition, β-MNs can innervate both intrafusal and extrafusal muscle fibers. Innervation of the muscle by the MN occurs at the neuromuscular junction, consisting of the axon terminal and the end plate, a highly excitable region of the muscle fiber. Here, presynaptic vesicles are released, ultimately causing the shortening (contraction) of the muscle fiber.

Further classifications of α-MNs differentiate between MNs that innervate fast twitch muscle fibers (F-type) and slow twitch muscle fibers (S-type). Slow twitch muscle fibers have a slower contraction time, a higher resistance to fatigue, and contain high amounts of mitochondria and myoglobin, which causes its reddish color (Burke, 1967; Eccles, Eccles, & Lundberg, 1958). In addition, S-type MNs have smaller somas when compared to F-Type (Granit, Phillips, Skoglund, & Steg, 1957). Fast twitch muscle fibers, conversely have a faster contraction time, lower resistance to fatigue, and contains lower amounts of mitochondria and myoglobin, which results in its pale color (Burke, 1967). F-Type MNs have a shorter AHP phase (50-110ms) and have a faster firing rate (Eccles et al., 1958). The ability to fire multiple action potentials quickly is correlated with a faster contraction of the innervated muscle. S-type MNs have a longer AHP phase

(>130ms), and exhibit a firing rate with a slower frequency and slower muscle contraction than F-type MN (Eccles et al., 1958). Postural muscles are innervated by a higher proportion of S-type MNs, which is advantageous due to their resistance to fatigue and slow contraction.

B1. Peripheral Nerve Injury: Introduction

Peripheral nerve injury refers to damage to the axon of a neuron in the peripheral nervous system. The most common instances of peripheral nerve injury occur via blunt trauma or penetrating wounds, most often the product of motor vehicle accidents and sports injuries (Eser et al., 2009).

Peripheral nerve axotomy leads to degeneration of the distal nerve stump within 48 to 96 hours s referred to as Wallerian degeneration (WD). During WD, a change in metabolic priority from production of neurotransmitters in the cell body to production of structural materials needed for axon repair and growth occurs. A microenvironment around the regenerating axon is created that allows successful regrowth of nerve fibers from the proximal nerve segment. In most instances, the zone of injury also extends proximally from the injury site to the next node of Ranvier, but death of the cell body itself may occur, depending on age and the site of injury (S. K. Lee & Wolfe, 2000). Schwann cells respond to loss of axons by extrusion of their myelin sheaths, downregulation of myelin genes, dedifferentiation and proliferation. Next, they align in tubes called Bungner bands, and express surface molecules that guide regenerating fibers (Stoll & Muller, 1999). Hematogenous macrophages are rapidly recruited to the distal stump and remove the vast majority of myelin debris (Stoll & Muller, 1999). Molecular

changes in the distal stump include upregulation of neurotrophins, neural cell adhesion molecules, cytokines and other soluble factors and their corresponding receptors (Fenrich & Gordon, 2004). Upon reestablishment of axonal contact, Schwann cells remyelinate nerve sprouts and downregulate surface molecules characteristic for precursor/premyelinating or nonmyelinating Schwann cells (Stoll, Reiners, Schwendemann, Heininger, & Toyka, 1986).

While both nerve crush and transection induce WD, there is an important difference in the probability of successful regeneration. A crush injury retains the continuity of the basal lamina, which provides guidance for regenerating axon from the proximal nerve stump to their targets. Hence, with a crush injury, successful reinnervation is expected after regeneration of the axon.

B2. Peripheral Nerve Injury: Motoneuron Survival

Two key factors determine MN survival following axotomy: location of injury and age. Proximal axon injury causes higher MN death rate than distal axon injury (Dai, Kanoh, Li, & Wang, 2000). Additionally, the survival rate of newborn MNs is much lower than that of adult MNs following axonal injury (Y. M. Chan, Wu, Yip, & So, 2002).

Following axotomy, MNs increase protein and mRNA expression necessary to promote nerve growth. This increase reaches a maximum after three days post-injury and returns to normal after three weeks. These proteins and mRNAs include the receptor for BDNF and NT-4, as well as NGF-R and trkB mRNA (Fenrich & Gordon, 2004). In the distal stump a number of neurite outgrowth-promoting molecules are upregulated. Nerve

regeneration occurs from the proximal stump at a rate of 3-4 mm/day after crush and 2-3 mm/day after sectioning a nerve (Fugleholm & Schmalbruch, 1994). Upon axonal regrowth, target organs are finally reached and muscle and skin are reinnervated. This occurs with specificity as motor axons preferentially reinnervate motor pathways after injury to mixed sensory-motor nerves (Madison, Archibald, & Brushart, 1996). After nerve transection myelinating Schwann cells previously associated with MNs differ from those Schwann cells that had myelinated sensory axons by their ability to express specific adhesion molecules when contacted by motor axons (Madison et al., 1996). This expression during critical stages of reinnervation provides an advantage for motor axons regenerating into the appropriate muscle pathways over those regenerating into the inappropriate sensory pathways.

Several studies focused on the responses of adult cat neck MNs to axotomy. In contrast to other MNs, 11-17 weeks after injury, the dendrite area increased, the total number of dendritic branches increased, and growth cone-like lamellipodia and filopodia formed (Rose & Odlozinski, 1998). 8-12 weeks post injury axon-like structures formed from distal MN dendrites, and 20- 35 weeks post injury some of these axon-like structures acquired synaptic connections (MacDermid, Neuber-Hess, & Rose, 2003). Permanent transection of motor nerve may cause a gradual elimination of whole axon collateral system in injured spinal motoneurons (Havton & Kellerth, 1990).

B3. Peripheral Nerve Injury: Physiological Changes

After peripheral nerve injury, short of transection, loss of functions include: motor control, proprioception, touch, temperature, and pain (S. K. Lee & Wolfe, 2000). Motor

control deficiencies, after injury, are further defined as a loss of fine motor control and areflexia. After denervation, distal structures undergo many changes. In major peripheral nerve injuries, osteoporosis may develop, and joints and soft tissues can become fibrotic and stiff (Burnett & Zager, 2004). In addition, the innervated muscle can atrophy and undergo interstitial fibrosis. As fibrosis progresses, the chances of functional reinnervation diminish if the nerve does not reach the motor endplates within approximately 12 months of denervation (Burnett & Zager, 2004).

In the cat, peripheral self-reinnervation occurs rapidly, however MN properties still remain altered and require more time to recover (Foehring & Sypert, 1986). After sectioning and resuturing of the MG nerve low reinnervation was observed after 5-6 weeks, however there were no differences between MNs that elicited muscle contraction and those that did not. After 9-10 weeks, motor units reversed their normal electrical properties with a slight increase in firing rate (Foehring & Sypert, 1986). Following long term reinnervation, 10% of MG MNs elicited no contraction of the MG muscle, however the electrical properties in the remaining MG MNs as well as the proportion of each motor-unit type returned to control levels (Foehring & Sypert, 1986; Foehring, Sypert, & Munson, 1986).

The difference between cross and self-reinnervated muscles has also been studied. Self-reinnervated hindlimb muscles in the cat, flexor digitorum longus and soleus, exhibit normal locomotor activity patterns (Dum et al., 1985). Interestingly, cross-reinnervated hindlimb muscles exhibited locomotor activity patterns associated with the innervating foreign MNs, suggesting that MN activation and input patterns remain unaltered centrally (Dum et al., 1985).

After reinnervation of the peripheral nerve to its target, motor performance is altered. In the human hand, orderly recruitment of muscle units is absent after injury (Thomas, Stein, Gordon, Lee, & Elleker, 1987). After reinnervation, motor unit recruitment again follows the size principle as long as the MNs reinnervated the same muscle or a close synergist. This recruitment pattern is also recovered after reinnervation of the MG nerve to its muscle in the cat (T. C. Cope & Clark, 1993).

A number of intrinsic MN properties are affected within a few days following axotomy. The rheobase, which is the minimum amount of current required to induce an action potential decreases, while the EPSP increases (Bichler, Carrasco, Rich, Cope, & Pinter, 2007a; Bichler et al., 2007b; Miyata & Yasuda, 1988; Nakanishi, Cope, Rich, Carrasco, & Pinter, 2005) The conduction velocity was shown to decrease, and its ramifications are discussed below (Gustafsson & Pinter, 1984a; Kuno, Miyata, & Muñoz-Martinez, 1974a).

B4. Peripheral Nerve Injury: Physiological Changes of Different Motor Unit Types

The relationship between the MNs and the muscles they innervate has been well established. The amount of recruited MNs and the MN firing rate are the determining factors controlling muscle force (Gossen, 2003). A faster frequency of action potentials or spikes has been correlated with a faster muscle twitch or contraction (Gossen, 2003). The determinant of this frequency is determined by the AHP, which is inversely correlated with the conduction velocity (Eccles et al., 1958; Gossen, 2003; Kuno, Miyata, & Muñoz-Martinez, 1974a). Hence, there is a positive correlation between motor unit contraction and the duration of AHP in both small mammals as well as humans.

Variations between the AHP and firing rate allow for the appropriate frequency of muscle contraction for a specific task. Following axotomy, electrophysiological recordings in cat F-type lumbar α-MNs has demonstrated an increase in AHP, MN input resistance, and membrane time constant (Kuno, Miyata, & Muñoz-Martinez, 1974b). The opposite effect may occur in S-type MNs (Kuno, Miyata, & Muñoz-Martinez, 1974b).

Interestingly, it was observed that the voltage response of MNs to a constant subthreshold hyperpolarizing current step reached a peak and decayed there after to a lower steady-state value (Gustafsson & Pinter, 1984b). The amplitude of this decay was found to be related to the AHP duration, such that cells possessing brief AHP durations exhibited the largest effect (Gustafsson & Pinter, 1984b). This influence was termed 'sag' process due to the nature of its effect on the membrane potential. Using these findings, a compartmental model demonstrated an inverse correlation between sag current and AHP duration (Gustafsson & Pinter, 1985). Finally, it was discovered that there was in fact a decrease in sag current in response to axotomy (Gustafsson & Pinter, 1985). These properties were also recorded following reinnervation (Kuno, Miyata, & Muñoz-Martinez, 1974b). After reinnervation, AHP and the conduction velocities returned to normal (Kuno, Miyata, & Muñoz-Martinez, 1974b). The degree of restoration of MN properties to control was related to the degree of reinnervation (Kuno, Miyata, & Muñoz-Martinez, 1974b). However, it was also observed that the degree of recovery of the MN properties was approximately the same regardless of the presence or absence of functional motor connections (Kuno, Miyata, & Muñoz-Martinez, 1974b).

A disturbance in the firing rate via a change in the AHP duration following axotomy, will alter muscle twitch and contraction and can cause a series of symptoms observed after peripheral nerve injury.

B5. Peripheral Nerve Injury: Synaptic stripping and changes in afferents

Some of the observations of axotomized MNs, may occur by alterations to properties extrinsic to the MN itself. For example, axotomized MNs lose synaptic contacts around the cell soma in a process known as "synaptic stripping" (Blinzinger & Kreutzberg, 1968; Sumner & Sutherland, 1973). Some, but not all, of these synaptic contacts are recovered with reinnervation (Blinzinger & Kreutzberg, 1968; D. Chen, 1978; Kellerth & Brannstrom, 1998; la Cruz & Pastor, 1994; Sumner, 1975).

Despite regeneration of muscle afferents in the cat and rat, self-reinnervated hindlimb triceps surae muscles exhibit significantly reduced stretch reflexes. (Cope, Bonasera, & Nichols, 1994; Haftel et al., 2005). Additionally, force production in self-reinnervated hindlimb muscles was restored, while response to the muscle stretch was not (Haftel et al., 2005).

Ia afferent neurons are sensory fibers that innervate muscle spindle receptors. These neurons are responsible for the monosynaptic stretch reflex via synapses on the α-MN based on changes in stretch Ia afferent fibers (Lüscher & Clamann, 1992). The Ia afferent synapses are glutamatergic and can be visualized by VGLUT1 immunoreactivity (Bellocchio, Reimer, Fremeau, & Edwards, 2000; Fyffe, 2001). It was shown that VGLUT1-immunoreactive synaptic boutons presumed to arise from muscle spindle primary afferents were lost proximally and shrunken distally on MNs in parallel with

retraction of the central projections of spindle afferent collateral axons from lamina IX (LIX) (Alvarez et al., 2011). This retraction occurred within days after nerve injury and was sustained despite nerve regeneration and reinnervation to the skeletal muscle (Alvarez et al., 2011). Regeneration did not restore collateral axonal projections into spinal LIX motor pools from afferents exhibiting normal muscle spindle-like responses to muscle stretch either (Alvarez et al., 2011). This study suggests the possibility that major changes in synaptic composition could produce different ratios of excitatory and inhibitory synapses. Without functional compensation by surviving synapses, restoration of normal muscle stretch reflexes and normal limb coordination would fail after regeneration, due to the permanent loss of feedback via stripped Ia afferent contacts. This synaptic disassembly, and the lack of reconnection of some Ia afferents with the muscle spindles provides a reasonable explanation for the reduction in monosynaptic transmission and the stretch reflex (Bullinger et al., 2011)

C1. HCN Channels: Introduction

As previously mentioned, permanent deficits to motor control are sometimes observed following reinnervation. These deficits are described as problems in the strength and timing of muscle contraction. Because firing rate directly determines muscle twitching, AHP, which determines the frequency of the firing rate, is of particular importance. Studies in the cat have shown that AHP is prolonged in F-type MNs and that this increase in duration is correlated with an increase in sag current amplitude. Because HCN channels underlie sag current, this thesis will attempt to analyze HCN immunoreactivity to determine the correlation between HCN expression with sag current.

Hyperpolarization-activated cyclic-nucleotide gated (HCN) channels were first discovered in the heart and are encoded by four genes (HCN1 – 4) that are widely expressed throughout the heart and the central nervous system (Milligan, Edwards, & Deuchars, 2006; Moosmang et al., 2001; Shi et al., 1999). In the rat central nervous system HCN1 is expressed in the neo-cortex, hippocampus, cerebellar cortex, brainstem and spinal cord (Milligan et al., 2006). HCN2 is distributed ubiquitously throughout most brain regions with the highest expression in the thalamus and brainstem nuclei, HCN3 is sparsely distributed at very low levels in the central nervous system with moderate to high expression only in the olfactory bulb and in some hypothalamic nuclei (Notomi & Shigemoto, 2004). HCN4 is strongly expressed in various regions of the brain such as the thalamic nuclei and in the mitral cell layer of the olfactory bulb (Notomi & Shigemoto, 2004). In the peripheral nervous system all four HCN subtypes have been reported in the dorsal root ganglion, with HCN1 being most abundant (Chaplan, Guo, Lee, & Luo, 2003).

All four HCN channel isoforms have been detected in heart. The expression levels of these isoforms strongly depend on the cardiac region and vary between species. In the sinoatrial node, in all species analyzed so far (e.g. rabbit, guinea pig, mouse and dog) HCN4 is the major isoform, accounting for about 80 % of I_h (Moosmang et al., 2001). The remaining fraction of this current is species-dependent. In rabbit, this fraction of I_h is dominated by HCN1, while in mice, HCN2 accounts for this fraction. So far, no data on the expression of HCN channels in human sinoatrial node are available.

The kinetics for voltage-dependent activation also differs between the HCN channel subtypes with HCN1 being the fastest, HCN4 being the slowest, and HCN2 and

HCN3 activating between HCN1 and HCN4 (Ludwig et al., 1999; Santoro, Liu, Yao, Bartsch, & Kandel, 1998).

C2. HCN Channels: Properties

Numerous studies have described and classified the ion channels associated with a specific current. The I_h current in particular, is produced by HCN channels. HCN channels are cation channels belonging to the super-family of voltage-gated pore loop channels (Yu, 2005). I_h current was first discovered in the rabbit sinoatrial node for its critical importance to cardiac function, contributing to the rhythmicity of the heartbeat, and as such has been termed the "pacemaker current" (H. Brown & DiFrancesco, 1980; Noma & Irisawa, 1976; Yanagihara & Irisawa, 1980). I_h current is also critical to neuronal function by the HCN channels unique property of a reverse voltage-dependence that leads to activation upon hyperpolarization (Bal & McCormick, 1997; Lüthi & McCormick, 1998; Maccaferri, 1996; H.-C. Pape & McCormick, 1989). Unlike most potassium channels, HCN channels are inwardly rectifying at rest due to a reversal potential of approximately -30mV, allowing for the passage of potassium ions and under certain conditions, sodium ions with a permeability ratio of 4:1 for potassium and sodium ions (D. DiFrancesco, 1986). Hence, I_h channels limit the extent of hyperpolarization during an action potential and can contribute to postinhibitory rebound. Through these properties, I_h contributes to several other neuronal processes, including burst firing, dendritic integration, synaptic transmission, and resting membrane potential (Robinson & Siegelbaum, 2003).

C3. HCN Channels: Physiological role

I_h is inwardly directed at rest and, hence, depolarizes the membrane potential upon activation. However, unlike the vast majority of cellular conductance that are activated upon membrane depolarization, I_h is activated by hyperpolarizing voltage steps to potentials negative to -70 mV, near the resting potential of cells (Robinson & Siegelbaum, 2003). Additionally, activation of I_h is facilitated by cAMP in a direct, protein kinase A -independent fashion, shifting the voltage activation of HCN channels to a more depolarized value (Altomare et al., 2003; Wainger, DeGennaro, Santoro, Siegelbaum, & Tibbs, 2001; J. Wang, Chen, & Siegelbaum, 2001). At voltages near the resting membrane potential, HCN channels are partially open, passing a depolarizing inward-current and as a result, sets the membrane potential to more depolarized values(Doan, 1999; Ludwig et al., 2003; H. Pape, 1996). This property reduces membrane resistance, which consequently reduces the change in membrane potential from any given input current than in the absence of HCN channels (Doan, 1999; Ludwig et al., 2003; H. Pape, 1996). The properties of HCN channels allow for the stabilization of membrane potential by opposing depolarizing or hyperpolarizing inputs. Upon hyperpolarization, HCN channels open, causing a depolarizing current and drives the membrane potential towards the reversal potential of the HCN channels and thus to a value closer to the resting membrane potential. As previously mentioned, the I_h current in this scenario is also termed voltage sag current. Upon depolarization, HCN channels close, eliminating the depolarizing current that was active at rest, thus contributing to a return of membrane potential to resting membrane potential (Biel, Wahl-Schott, Michalakis, & Zong, 2009). This quality underlies many of HCN channel's

physiologically significant properties, such as pacemaking in cardiac myocytes and thalamocortical relay neurons.

Studied extensively in the CA1 hippocampal and neocortical pyramidal neurons, is the role of I_h in the kinetic filtering. Due to passive cable properties, EPSPs from distal inputs should theoretically be of lesser amplitude and decay slower than proximal EPSPs. Slower decay allows for the summation of overlapping voltage changes caused by other synapses. However, electrophysiological studies have shown that EPSP amplitude and temporal integration is independent of input distance (Magee, 2000). Although the lack of attenuation for the amplitude of EPSPs is caused by another mechanism (increased density of AMPA-type glutamate receptors at distal dendritic synapses) the kinetic filtering property of HCN1, that is the gradient of HCN channels increases from proximal to distal dendrites, is responsible for the shortening time constants of distal EPSPs (Magee, 2000). The presence of I_h in the distal dendrites is thought to modify the EPSP time course by enhancing the local resting membrane conductance, thereby providing a leakage path for current flow that decreases the local membrane time constant and hence speeds the decay of the distal EPSP (Magee, 2000). By normalizing the time course of the EPSP, I_h presumably increases the information processing capabilities of the dendritic tree, permitting distal and proximal EPSPs to carry similar temporal information content (Magee, 2000).

In addition to unique activation kinetics, a unique paradoxical effect in EPSP attenuation has been observed in HCN channel. I_h can generate an excitatory inward current that exerts a direct depolarizing effect on the peak voltage of weak EPSPs, yet produces a paradoxical hyperpolarizing effect on the peak voltage of stronger, but still

subthreshold, EPSPs (George, Abbott, & Siegelbaum, 2009). The inhibitory action of I_h is caused by its interaction with the delayed-rectifier M-type K^+ current (George et al., 2009). Despite the fact that I_h provides a depolarizing current at subthreshold potentials, results from several studies indicate that it has a paradoxical inhibitory effect on the ability of an EPSP to trigger an action potential, beyond its intrinsic properties of increasing resistance (George et al., 2009). In this manner, I_h can enhance spike firing in response to an EPSP when spike threshold is low and can inhibit firing when spike threshold is high (George et al., 2009).

In the auditory brainstem, I_h current influences the resting membrane potential and can delay the generation of action potentials in response to injected current (R. N. Leao et al., 2006b). I_h current increases rebound depolarizations following hyperpolarizations and increases the likelihood of rebound action potentials (K. E. Leao, Leao, Sun, Fyffe, & Walmsley, 2006a).

The unique properties of HCN channels have also led I_h current to be termed sag current. I_h current will actively oppose hyperpolarizations. For this reason, it has an effect on the afterhyperpolarization (AHP) phase. The duration of the AHP is inversely correlated with the amplitude of sag current (Gustafsson & Pinter, 1984a). Hence, the greater in amplitude the sag current, the shorter AHP duration will be. Consequently, the length of AHP determines the frequency of the firing rate. I_h current contributions to AHP and postinhibitory rebound characterize the role of HCN channels and rhythmic bursting.

MNs, during locomotion, exhibit membrane potential oscillations between hyperpolarization and depolarization phases via changes in the rhythmic balance between

synaptic excitation and inhibition corresponding to the onset of muscle activity (Gorassini, Bennett, & Kiehn, 1999). Using the HCN channel blocker of ZD7288 or CsCl, the contribution of I_h to MN activity during locomotion can be assessed. When the I_h current was blocked in the rat, MNs hyperpolarized indicating that I_h is tonically active at rest in rat motor neurons (Kiehn, Kjaerulff, Tresch, & Harris-Warrick, 2000). Tonic I_h activation also explains the observation that ZD 7288 increased resting input resistance (Kiehn et al., 2000). Replacement of I_h decreased the time for phase transition between the inhibitory and excitatory phases, decreased time to the first action potential in the locomotor cycle, and increased the mean firing frequency throughout the cycle (Kiehn et al., 2000). These observations are compatible with the idea that $I_{h,}$ contributing to an inward, depolarizing current, helps the cell escape from inhibition faster than when I_h is absent. It also shows that the depolarizing rebound caused by the slow deactivation of I_h phase advances cyclic spiking. These findings demonstrate that the role of rhythmic activity by HCN generated current found in other areas of the nervous system are consistent with its role in shaping of MN activity (Kiehn et al., 2000).

C4. HCN Channels: Nervous system diseases and channelopathies

Epilepsy is characterized by a chronic recurrence of unprovoked seizures. These seizures are usually symptoms of abnormal, excessive or synchronous neuronal activity in the brain. Altered expression levels of the HCN channels have been demonstrated in hippocampus of patients with severe temporal lobe epilepsy as well as in animal models of temporal lobe and absence epilepsies (Richichi et al., 2008).

In a mouse model for the neurodegenerative disorder of Parkinson's disease, a profound motor disability occurs that is traceable to a decline in synchronous and rhythmic spiking in the neurons of the external segment of the globus pallidus (C. S. Chan et al., 2010). As this loss was traceable to the downregulation of HCN channels, viral delivery of HCN restored the rhythmic spiking (C. S. Chan et al., 2010).

These diseases and channelopathies demonstrate the profound impact of downregulation or a loss of HCN channel expression can have in the nervous system. These HCN-related diseases usually manifest into alterations of rhythmic spiking, due to the role of HCN channels in pacemaking and neuron excitability. The location of downregulation usually defines the unique symptoms attributed to the disease.

Knockout studies of HCN channels have recently been used to determine the role of I_h current in Long-term potentiation (LTP), working memory, and motor learning(Baruscotti, Bottelli, Milanesi, DiFrancesco, & DiFrancesco, 2010).

C5. HCN Channels: Regulation

All of the isoforms of HCN have a voltage-dependent activation at hyperpolarized values to the resting membrane potential, however each isoform has a unique midpoint of activation value. These values are –70 mV, –95 mV, –77 mV to –95 mV and –100 mV for HCN1, HCN2, HCN3 and HCN4 respectively (Altomare et al., 2003; Baruscotti, Bucchi, & DiFrancesco, 2005). As their name suggests, HCN channels are also regulated by cyclic nucleotides, specifically, cyclic AMP (cAMP) (Altomare et al., 2003; Wainger et al., 2001; J. Wang et al., 2001). cAMP speeds up the opening kinetics by shifting the activation curves of HCN2 and HCN4 by about +10 to 25 mV (Altomare et al., 2003;

Wainger et al., 2001; J. Wang et al., 2001). HCN1 and HCN3 exhibit, if at all, only a weak response to cAMP (Altomare et al., 2003; Wainger et al., 2001; J. Wang et al., 2001).

In addition to cAMP other factors have been shown to contribute to the shift in voltage dependence of HCN channels including p38-MAP (mitogen activated protein)-kinase, tyrosine phosphorylation, proton concentration, and PIP2 (phosophatidylinositol-4,5-bisphosphate)(Pian, Bucchi, Robinson, & Siegelbaum, 2006; Poolos, Bullis, & Roth, 2006; Zolles et al., 2006). For example, PIP2 is an allosteric ligand that increases the voltage-dependence of HCN channels by approximately 20mV, resulting in a much more physiologically relevant voltage-activation range (Pian et al., 2006; Poolos et al., 2006). Consequently, enzymatic degradation of phospholipids reduces channel activation and slows down firing frequency of neurons (Pian et al., 2006; Poolos et al., 2006).

C6. HCN Channels: Heteromeric co-assembly

In addition to the unique characteristics of the HCN isoforms is the ability to form heteromeric structures (Altomare et al., 2003; Brewster, Bernard, Gall, & Baram, 2005). Heteromeric assembly is defined by the combination of subunits from different isoforms. This was first discovered with respect to the HCN channels in the rabbit sinoatrial node (Altomare et al., 2003). Additionally, a heteromeric HCN1/HCN2 channel was discovered in the rat hippocampus (Brewster et al., 2005). In this case, the presence of the heteromeric structure was found to promote hippocampal hyperexcitability and result in epilepsy and seizures (Brewster et al., 2005). The characteristics of the heterocomeric

structure are borrowed from its homomeric constituents and can be identified electrophysiologically (Brewster et al., 2005; C. S. Chan, 2004).

C7. HCN Channels: Motoneuron significance

As previously mentioned, various intrinsic properties of α-MNs are altered after denervation. It has been clinically observed that full functional motor control is not complete following reinnervation. Furthermore, the full effect of reinnervation on the recovery of MN properties has yet to be defined. HCN channels, which underlie I_h (sag current), are responsible for the rhythmic firing and bursting in the cells in which they are expressed. They are also responsible for much of the intrinsic properties of α-MNs that are altered following peripheral nerve injury such as conduction velocity and AHP. In addition, a tonic depolarizing I_h current at rest also decreases membrane resistance and will attenuate EPSPs and MN recruitment. Conversely, a decrease in I_h current will increase EPSP amplitude, an observation seen within a few days following peripheral crush injury (Miyata & Yasuda, 1988). The expression or immunoreactivity of HCN channels in the α-MNs following peripheral nerve injury has not yet been assessed.

Hypothesis:

In this thesis, we investigate whether or not HCN channel immunoreactivity alters with injury. Additionally, we will study whether or not reinnervation affects HCN immunoreactivity. Because HCN channels underlie sag current, and sag current has been shown to decrease with injury, we hypothesize that HCN1 immunoreactivity will decrease following axotomy.

III. Aims

Aim 1 characterizes the expression and anatomical location of HCN channel isoforms in the adult rodent in α-motoneurons through immunoreactivity. In order to test the effect of injury, we first must characterize the expression of the HCN channels and its isoforms in lumbar α-MNs. This will allow us to determine which isoforms are expressed within the membrane and underlie sag current. To determine this, HCN channels were labeled in conjunction with known presynaptic and postsynaptic markers such as VAChT, VGlut1, VGlut2, KV2.1, 5-HT, Gephyrin, and Synaptophysin and analyzed for colocalization.

Aim 2 characterizes the developmental expression and location of HCN and its isoforms in α-motoneurons. Previously, our laboratory has characterized the emergence of sag current with postnatal age and adult-like locomotion. Determining the postnatal age that HCN channels are expressed will provide insight into a possible correlation with sag current, adult-like locomotion, and injury. It will also determine if different isoforms are preferentially expressed with development. *The specific hypothesis is that HCN channel expression will increase at the post-natal age of 14 days old (when rats demonstrate the locomotor abilities and sag current emerges) and continue to increase until full adult like locomotion is exhibited.* To test this hypothesis, immunolabeling of the HCN channels will be performed on rat lumbar spinal cord tissue of postnatal age 10d, 12d, 14d, 17d, 21d, and 28d.

Aim 3 determines the difference in HCN1 Immunoreactivity in S-type vs. F-Type α-Motoneurons. Characterizing the differences in HCN1 expression on MNs innervating different muscle types, will provide a correlation between HCN1-IR and AHP since F-type and S-type MNs exhibit different durations of AHP. In addition it will provide background for further studies analyzing the changes in HCN-IR between the two different MNs unit types. *The specific hypothesis is that F-Type MNs will exhibit higher HCN1 immunoreactivity since F-Type MNs exhibit a shorter AHP.* In order to test this hypothesis, dual retrograde labeling of MG/LG MNs and soleus MNs will be done with CTb-Green and CTb-Red respectively. A majority of soleus MNs are described as S-type and a majority of MG/LG MNs are described as F-Type. Injecting CTb-Green into the MG/LG muscle and CTb-Red into the soleus muscle will allow us to distinguish and compare HCN1 immunoreactivity in F-type vs. S-type MNs.

Aim 4 determines the effect of peripheral axonal injury on the expression of HCN1 proteins in the membrane of the soma and dendrites of α-motoneurons innervating the medial and lateral gastrocnemius. *The specific hypothesis is that HCN1 immunoreactivity will decrease following axon injury.* To test this hypothesis HCN1 immunoreactivity will be analyzed for the MN pool, the soma, and the proximal dendritic arbor following injury. In order to determine the influence of reinnervation on HCN channel expression, two different types of injury will be used. One set of rats will undergo a tibial nerve transection with the proximal end of the nerve ligated and prevented to reconnect with the distal end. The second set of rats will undergo a crushed

tibial nerve injury. These analyses will take place at various post-injury recovery time-points following the two different types of injury. In addition, sag ratio will be measured with electrophysiology of the α-MN to correlate the expression of HCN1-IR with sag current.

IV. Materials and Methods

A. Surgical Procedures

All animal procedures were performed according to National Institutes of Health guidelines and were reviewed by the local Laboratory Animal Use Committees at Wright State University. The data described, with the exception of specific aim 2 were obtained from adult Sprague Dawley rats that underwent different combinations of the procedures explained below.

All survival surgeries (i.e., nerve surgeries and tracer injections) and physiological recordings were obtained from rats deeply anesthetized by isoflurane inhalation (induction 4 –5%; maintenance 1–3%, both in 100% O2). After survival surgeries, the animals received subcutaneous injections of buprenorphine (0.1 mg/kg) immediately and every 12 h after surgery prophylactically to alleviate any possible pain and distress. Pain and distress were closely monitored but not observed in any of the rats. In terminal experiments, rats were transcardially perfused with fixatives for histological analyses as described below. This procedure was performed under the effects of a lethal overdose of or Euthasol (>50 mg/kg) and confirmation of deep anesthesia.

For specific aim 2, 1 rat was euthanized, perfused, and fixed at each postnatal age of 10d, 12d, 14d, 17d, 21d, and 28d. In specific aim 3, CTb-FITC was injected into the left MG/LG muscle and CTb-CY3 (red) was injected into the left soleus muscle, one week prior to euthanization. For specific aim 4, approximately 30 adult female Sprague

Dawley rats (200-350 g) underwent left tibial nerve crush or cut surgeries. CTb-FITC was injected into the left MG/LG muscle one week prior to crush or cut injury to allow for the retrograde labeling of injured MNs at seven different time points after the surgery (1-day, 3-day, 8-day, 2-week, 1-month, 3-month, and 6-month) Two rats were used at each time point in both cut and crush injury models. Two additional rats with sham injuries (tibial nerve was isolated and exposed but not injured) were euthanized, perfused and fixed at the 8-day and 1-month time point.

Retrograde Labeling

To retrogradely label MG/LG MNs, the left leg was shaved and cleaned with 70% ethanol and betadine. A small incision was made with a scalpel on the midline of the left leg and skin separated from the muscle using the dissection scissors. The incision was extended rostrally to the division of the biceps femoris and caudally down to the ankle. The biceps femoris was reflected and the connective tissue around the lateral and medial gastrocnemius cleared. A microsurgery retractor was used to secure the biceps femoris. Several 2-5 μL intramuscular injections of CTb-FITC at 0.1% were distributed evenly throughout the MG/LG muscle. Then the biceps femoris was closed using 4-O ethicon absorbable vicryl with a PS-5 needle in 3-4 sutures in an interrupted pattern. Then an interrupted subcutaneous closure of the skin was performed with surgical knots and irrigated with saline. For specific aim 3, CTb-FITC was only injected intramuscularly into the MG muscle and CTb-Cy3 was injected into the soleus muscle.

Nerve Injuries

Nerve injuries were performed by a midline incision (~2 cm) through skin, underlying connective tissue, and biceps femoris in the left hindlimb to expose the tibial

nerve at mid-thigh. For the cut and ligate surgery, tibial nerve was transected and the proximal stump of the cut nerve was immediately ligated with double tie. This tie prevented the injured axons from regenerating. For the crush injury, the tibial nerve was isolated and crushed for 5 seconds using jeweler forceps. After washing with 0.9% sterile saline the wound was closed in layers, and the animals removed from anesthesia underwent post- operative care as explained above. All survival surgeries were performed by Lori Goss, RVT.

B. Tissue preparations for analysis

Transcardial Perfusion with fixatives.

The animals were transcardially perfused and fixed with 4% Paraformaldehyde in 0.1 M phosphate buffer, pH 7.3 (PB). First, each animal was injected intraperitoneally (IP) with pentobarbital at 150mg/kg. Once deeply anesthetized, as indicated by lack of corneal and pineal reflexes, .05 mL of Heparin was injected retroorbitally into the bloodstream to prevent vascular clotting during the perfusion. The thoracic cavity was opened and resected. A perfusion cannula was then inserted into the left ventricle and an incision made in the right atrium for drainage. The perfusates were pulsed using a peristaltic pump. First 100-200 ml of vascular rinse was used to clear the vascular system. Then the fixative (4% paraformaldehyde in 0.1 M phosphate buffer saline solution), (200-300 ml for adults, 25-50 ml for postnatal) was passed through the vascular system. The spinal cord (T1-S1) was then dissected out and placed in the same fixative for 2 hours to overnight for post-fixation. The tissue was then cryoprotected by placing it into a solution of 15% sucrose in 0.1M PB at 4°C, overnight or until used.

Histological sectioning

The lumbar spinal cord was frozen in tissue freezing medium (OCT, Tissue Tek) and cut by a cryostat. Transverse sections of the lower lumbar spinal cord (L4 to L6) were cut at 50 μm thickness and collected free floating in 0.1 M PBS. All tissue sections were processed free-floating.

Immunohistochemistry

The sections were washed via pipette three times for 5 minutes each using 0.1 M phosphate buffered saline with 0.1% Triton X. Tissue was blocked using normal horse serum at diluted at a 1:10 concentration with 0.1 M phosphate buffered saline with 0.1% Triton X for at least thirty minutes. These sections were then incubated at 4°C overnight with the primary antibodies as listed in table 1.

The tissue was washed three times at 5 minutes each with 0.1 PBS with Triton X. Primary antibodies were visualized with Cy3, Cy5, and FITC secondary antibodies conjugated to their respective host. Nissl immunocytochemistry was performed using fluorescein-conjugated nissl, diluted using PBS with Triton X at 1:100 (Molecular Probes, Carlbad, CA). Slides were again washed with PBS with Triton X two times for 5 minutes followed by a washing with 0.1 M phosphate buffered saline two times for 5 minutes. The spinal cords were then mounted to gelatin-coated slides and cover slipped using Vectashield mounting medium (Vector Laboratories).

Table 1. Primary Antibodies used for Immunohistochemistry

Antibody	Dilution	Host	Manufacturer	Lot#
HCN1	1:200	Mouse	Neuromab	444-1LC
HCN1	1:100	Rabbit	Alomone	AN-09
HCN2	1:100	Rabbit	Alomone	AN-11
HCN4	1:100	Rabbit	Alomone	AN-14
VAChT	1:3000	Goat	Chemicon	LV1387923
VGlut1	1:5000	Guinea Pig	Synaptic Systems	135304/2
VGlut2	1:1000	Guinea Pig	Synaptic Systems	135404/11
5-HT	1:1000	Guinea Pig	Wright State University	N/A
Synaptophysin	1:300	Mouse	Synaptic Systems	12530031
Gephyrin	1:100	Guinea Pig	Boerhinger Mannheim	13108224
MAP2	1:250	Mouse	Upstate Biochem	0701049386

Western Blotting

Freshly dissected L4/L5 spinal cord region was dissected from adult Sprague Dawley rats. Samples were homogenized in .3M sucrose in .1M phosphate buffer at pH 7.4 containing 10mM Hepes, 1mM EDTA and Complete Mini protease inhibitor cocktail (Roche Applied Sciences, Indianapolis, IN) and phosphatase inhibitors, 10 mM NaF and 2 mM Sodium ortho-vanadate (Na3VO4) were used. The homogenate was centrifuged at 3000 x g for 10 minutes at 4°C to remove the nuclei. The supernatant was collected and ultracentrifuged at 100,000 x g for 1 hour at 4°C. The pellet or crude membrane fraction was resuspended in homogenization buffer. Protein concentration was determined by Bradford Reagent Assay (Bio-Rad, Hercules, CA) with bovine serum albumin as a standard.

SDS/Polyacrylamide gels and immunoblotting.

The membrane fraction was size fractionated on a 10% SDS- polyacylamide gel using Lauryl Sulfate (Sigma Cat#L5750, St. Louis, MO) as the SDS source. After electrophoretic transfer to PVDF membrane (Millipore, Billerica, MA), the resulting immunoblots were blocked in Blocker TM BLOTTO with 5% (w/v) nonfat dairy milk in 25 mm Tris, 150mm NaCl, pH7.4 (Pierce, Rockford, IL) overnight. The mouse anti-HCN1 obtained from the UC Davis/NINDS/NIMH Neuromab facility (Davis, CA) was diluted 1:500 in BLOTTO and incubated overnight at 4°C. After washing 4 x 10 minutes in Tris buffered saline (TBS), the immunoblot was incubated in HRP anti-mouse (Biomeda, Foster City, CA) for 1 hour and then washed in TBS 4 times for a total of 40

minutes. The blots were developed with ECL (Pierce, Rockford, IL) and imaged using a Fuji Bioimager 1000 (Stamford, CT).

Figure B. Western Blot of HCN1 antibody confirming specificity by a single defined band at 100 kDa

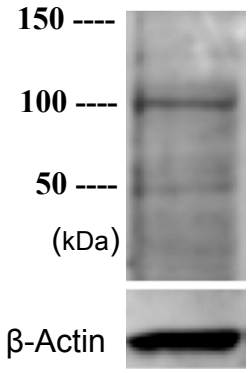

Electrophysiology

Standard operating procedures were used to prepare the spinal cord and the left hindlimb for electrophysiological stimulation and/or recording with the rat fixed in a rigid recording frame (Bullinger et al., 2011; Haftel et al., 2005). Exposure of tissues in the posterior compartment of the left hindlimb by skin incision gave access to the tibial nerve, which was carefully dissected free of other tissues and suspended in continuity on a monopolar silver hook electrode for electrical stimulation (at a site just rostral to the lesion site for rats in the regenerated group). In addition to its other uses, electrical stimulation of the tibial nerve in all treated rats yielded contraction of posterior compartment muscles, thereby verifying successful self-reinnervation. The common peroneal and sural nerves were crushed. The triceps surae muscles were freed of surrounding tissue, and their common tendon of insertion (Achilles tendon excluding the plantaris muscle tendon) was detached from the calcaneous and tied directly to the lever

of a motor system (model 305B-LR, Aurora Scientific). Dorsal exposure of the lumbosacral spinal cord (L4–S1) by laminectomy and longitudinal incision of the dura mater provided access to 1) dorsal roots L4,5, which were carefully dissected free of surrounding tissue and suspended in continuity on bipolar silver hook electrodes for recording, and 2) tibial motoneurons in L4,5 ventral horn via a dorsolateral penetration of the spinal cord. Skin flaps were used to construct pools for bathing all exposed tissues with warm mineral oil.

Motoneurons were impaled by borosilicate glass microelectrodes (1.2-mm OD, 7- to 10-MΩ DC resistance, 2 M K-acetate) advanced through the spinal cord with a micromanipulator system (Transvertex Microdrive). Tibial motoneurons were selected for study and identified by antidromic action potentials elicited by electrical stimulation of the MG peripheral nerve (current strength 2.5X muscle contraction threshold, pulse duration 40 μs). Only those motoneurons with stable membrane potential and with action potential amplitude >60 mV were deemed acceptable for study. Motoneurons were injected with hyperpolarizing current through the micropipette in order to measure sag current. Sag ratio was calculated by dividing the difference between the peak and the steady state potential by the difference between the peak and the baseline potential. All electrophysiology experiments for this thesis were performed by Adam S. Deardorff in the laboratory of Timothy C. Cope.

C. Imaging and Analysis

The slides were imaged and analyzed via FV1000 Confocal Microscope by Olympus and excited with line lasers of 405nm, 488nm, 568nm, and 633nm.

Spec*ific Aim3:*

S-Type MNs were designated as those retrogradely labeled with CTb-Cy3 and F-Type MNs as those labeled with CTb-FITC. The MNs intensity was determined by a trace of the MNs somatic membrane in a single optical section. This value was normalized by diving it by the neuropil background of the optical section containing the MN of interest. The neuropil background value was created by averaging intensities of four regions of the neuropil that did not contain a neuronal soma.

Specific Aim 4:

The injured side of the spinal cord was identified by the immunoreactivity of CTb-FITC (green) in the injured MNs. The injured and uninjured MN pools were imaged using a 20X objective and individual MNs were imaged using 60X oil objective and stacks of confocal optical sections separated by 1 μm z-steps collected throughout the thickness of the tissue section. Using Fluoview® software, intensity profiles of injured and uninjured MN pools of the same slice were measured. Additionally, intensity profiles from membrane and proximal dendrite traces were measured for individual injured and uninjured MNs of the same slice. Intensity values from injured MN pools, MN membrane, or MN dendrite were divided by the intensity values from its uninjured counterpart of the same spinal cord section to give a normalized value. These values were compared across time points and to values obtained from sham injuries.

Statistics

Statistical analysis and graphing were performed with Excel (Microsoft), Sigma Stat 3.1 (Jandel), and Sigma Plot 9 (Jandel). One way ANOVA and t-test were respectively used for comparisons between ligate and crush relative intensities for the same time point and pairwise comparisons between sham and injury relative HCN1 intensities. Significance level was set at $p<0.05$.

Figures

Images were composed using Fluoview (FV) software, Image Pro Plus 5.1, and Corel Draw 11. Sharpening of some images was performed by applying a High Gauss filter in Image Pro Plus 5.1. Images were digitally retouched for brightness, contrast, and gamma. None of the digital modifications altered the content of information within the images.

V. RESULTS

Aim 1:

Expression and anatomical location of HCN isoforms in lumbar α-MNs

This study focuses on the intrinsic MN properties that affect AHP, specifically, the amplitude of sag current that is correlated with AHP. As HCN channels underlie sag current, it was imperative to characterize the expression of the HCN isoforms. Determining this expression will provide the basis for what to expect and how to analyze HCN immunoreactivity (IR) following peripheral axotomy. IR of HCN channels was used to determine which HCN isoforms are expressed postsynaptically in the membrane of α-MNs and thus contribute to sag current. HCN antibodies were initially tested and confirmed for positive IR on cardiac tissue, where their expression has been established (Ludwig et al., 1999; Moosmang et al., 2001; Shi et al., 1999). The specificity for the monoclonal antibody of HCN1 was confirmed using a western blot. Specificity for HCN2 and HCN4 antibodies were confirmed using peptide blocks. Certain markers, whose location has been established, can be used to determine presynaptic or postsynaptic location. HCN1's postsynaptic expression has previously been confirmed via electron microscopy and IR (Milligan et al., 2006). Our labeling confirmed dense HCN1 labeling throughout the membrane, evenly outlining the neuronal soma (Figure 1A). In order to identify background and neuropil labeling, microtubule-associated protein (MAP2) was used in order to confirm dendritic labeling (Figure1B). HCN1-IR

was observed in proximal dendrites (those that branched off a neuronal soma within the optical section) as well as distal dendrites whose neuronal soma was not visible in the optical section. Studies in the neocortical pyramidal neurons have demonstrated HCN1 expression in both distal and proximal dendrites (Magee, 2000). Finally, slight HCN1-IR was visible within the cytoplasm where protein channel synthesis and trafficking occur.

Previously unreported, however, is the presence of the HCN2, HCN3, and HCN4 isoforms in the lumbar lamina IX of the spinal cord. Previous studies of HCN3 expression have reported sparse expression in the olfactory bulb, hypothalamic nuclei, and sinoatrial node (Notomi & Shigemoto, 2004), however, the HCN3 antibody did not express positive IR in the region of α-MNs and was left out of the following experiments. Isoforms HCN2 and HCN4 did express positive IR in the region of α-MNs. In order to determine the precise localization (presynaptic vs. postsynaptic) of HCN2 and HCN4, Kv2.1 (a voltage gated potassium channel and known postsynaptic marker) and synaptophysin (a synaptic vesicle protein and known presynaptic marker) were labeled in conjunction with HCN2 and HCN4. Line intensity analysis was used to determine if colocalization was present indicating the location of HCN2 and HCN4. HCN2 IR is presynaptic to MNs, as revealed via colocalization with synaptophysin and not Kv2.1. Vesicular acetylcholine transporter (VAChT) is a presynaptic cholinergic marker. A majority of HCN2 clusters exhibited colocalization with VAChT (Figure 3). Clusters of HCN2 that were not colocalized with VAChT were colocalized with VGlut1, a presynaptic glutamatergic marker of Ia afferents. Additional markers that were not colocalized with HCN2-IR include Gephyrin, 5-HT, and VGlut2. HCN4 demonstrated colocalization with Kv2.1, a postsynaptic marker (Figure 4) suggesting that MNs do

express this isoform in addition to HCN1. However, our labeling of HCN4 was not consistent among multiple samples of α-MNs. HCN4 did not colocalize with VAChT, VGlut1, VGlut2, Synaptophysin, or 5-HT. Thus, HCN2-IR is expressed presynaptic to the membrane and HCN4-IR is expressed with the membrane. This thesis will focus on HCN1-IR, which exhibited robust, precise labeling within the membrane of all α-MNs.

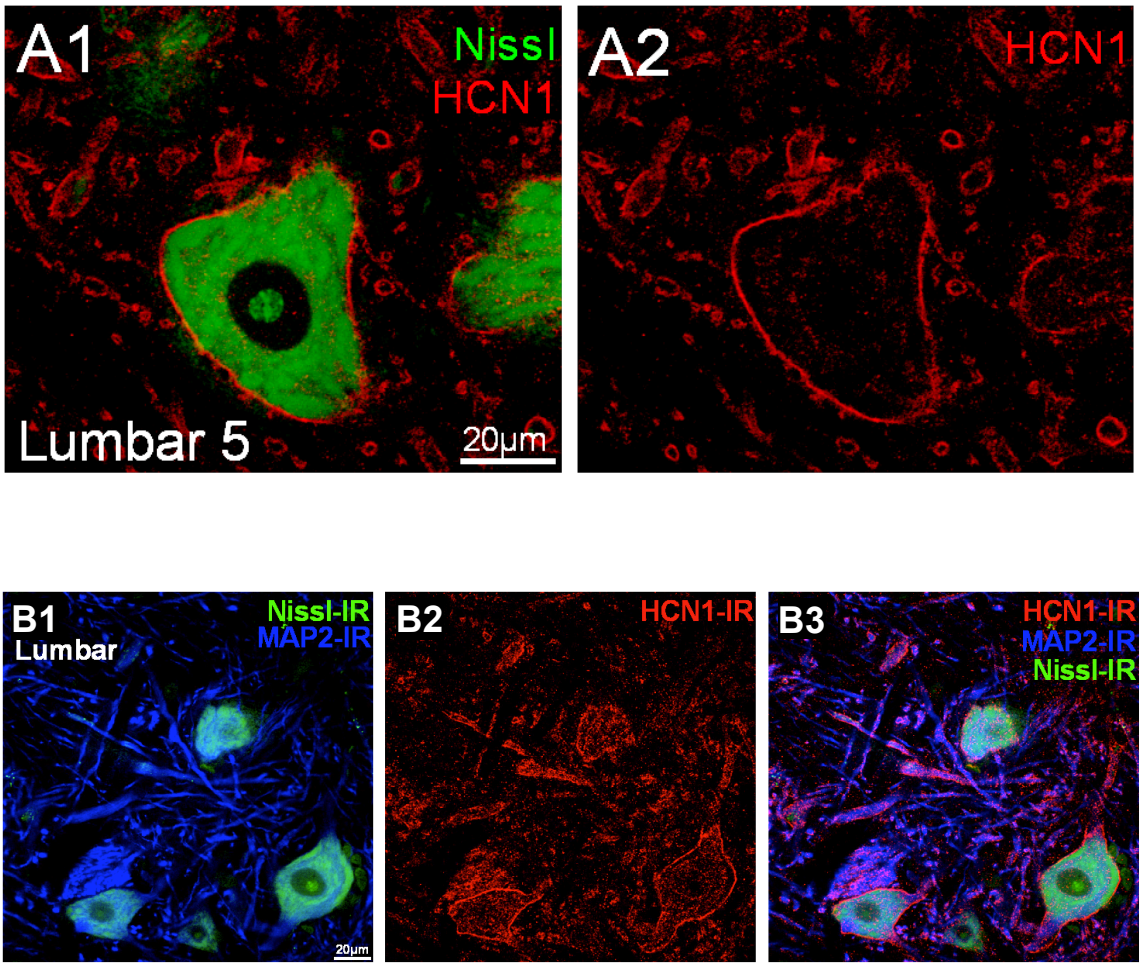
A1
Nissl
HCN1
Lumbar 5
20μm
A2
HCN1
B1
Lumbar
Nissl-IR
MAP2-IR
20μm
B2
HCN1-IR
B3
HCN1-IR
MAP2-IR
Nissl-IR

Figure 1. HCN1 immunoreactivity in the membrane and proximal dendrites of lumbar α-motoneurons. HCN1-IR in red is observed around the membrane of lumbar α-MNs (A1,A2). In addition, HCN1-IR is observed along the dendrites, labeled with MAP2 in blue (B3). Nissl label in green is used as a neuronal stain.

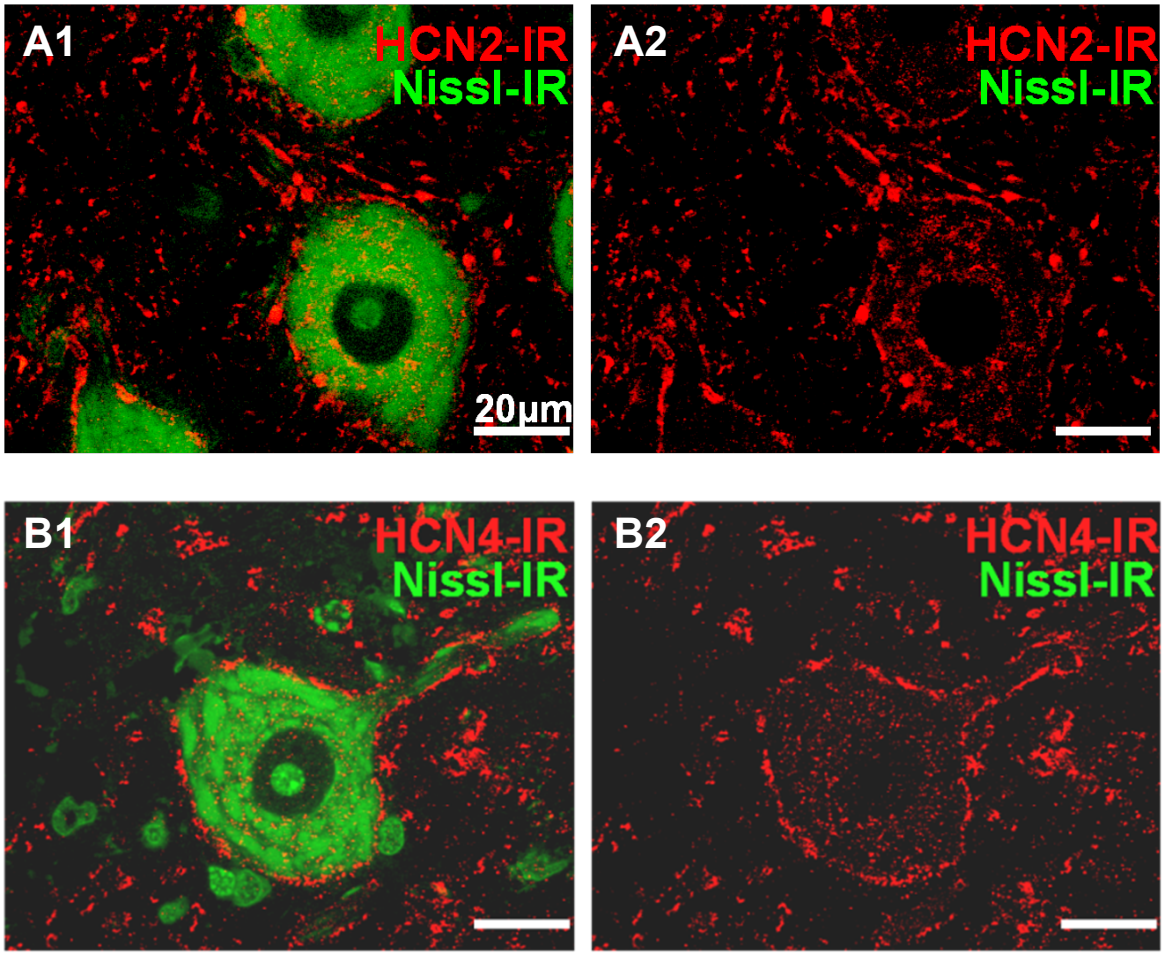
A1
HCN2-IR
Nissl-IR
20μm
A2
HCN2-IR
Nissl-IR
B1
HCN4-IR
Nissl-IR
B2
HCN4-IR
Nissl-IR

Figure 2. α-MNs express HCN2-IR and HCN4-IR. Both HCN2 in red (A) and HCN4 in red (B) exhibit positive IR around lumbar α-MNs. Unlike, HCN1, the expression and location e.g. postsynaptic expression or presynaptic expression to the membrane of HCN2 and HCN4 has yet to be determined. Nissl label in green is used as a neuronal stain.

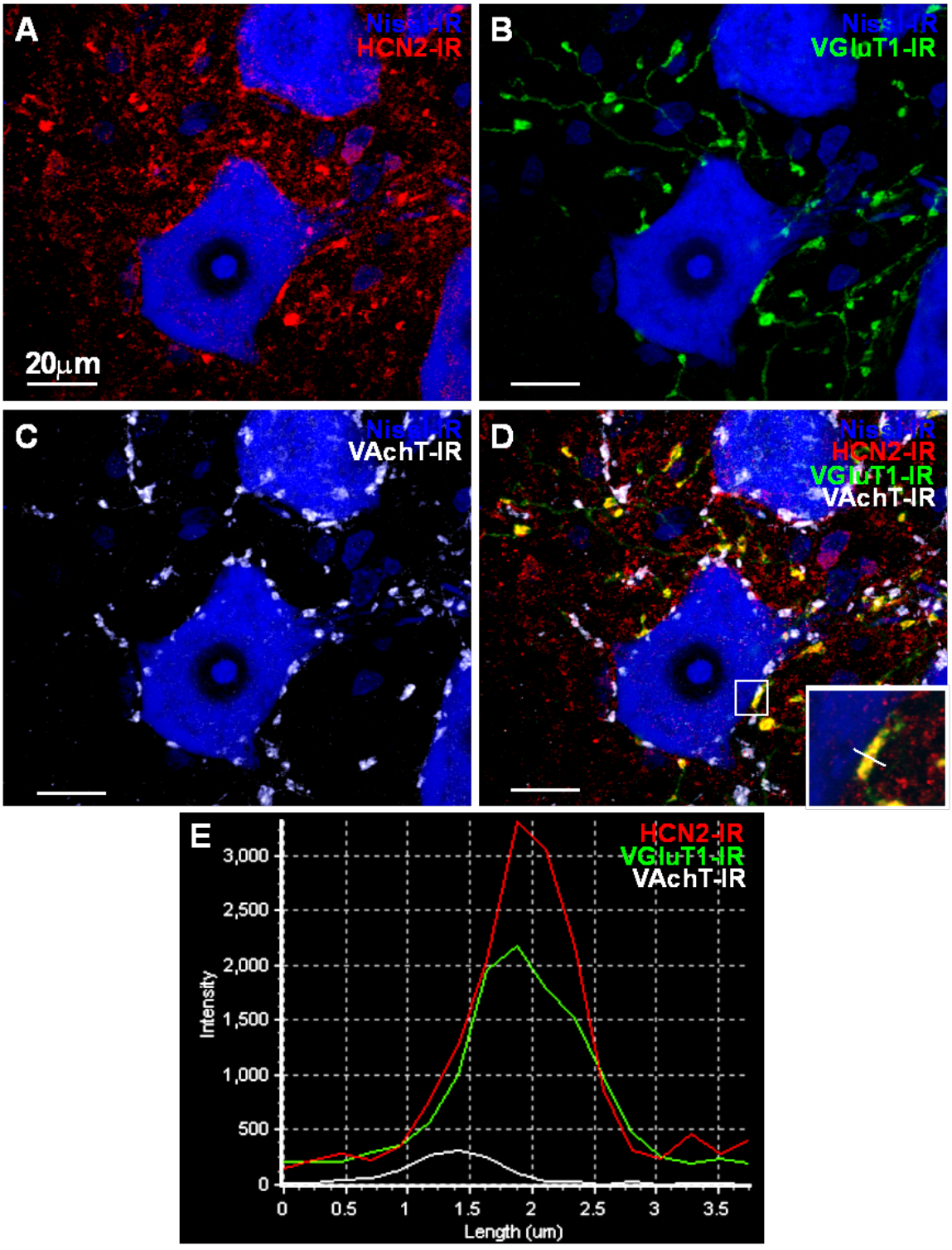
A
Nissl-IR
HCN2-IR
20μm
B
Nissl-IR
VGluT1-IR
C
Nissl-IR
VAchT-IR
D
Nissl-IR
HCN2-IR
VGluT1-IR
VAchT-IR
E
HCN2-IR
VGluT1-IR
VAchT-IR
Intensity
3,000
2,500
2,000
1,500
1,000
500
0
0
0.5
1
1.5
2
2.5
3
3.5
Length (um)

Figure 3. HCN2-IR colocalizes with VAChT-IR and VGlut1-IR presynaptic contacts and is not located within the α-MN membrane. IR for HCN2 was analyzed in conjunction with VAChT and either Kv2.1, VGlut1, VGlut2, Gephyrin or Synaptophysin. A line intensity scan was used to determine if expression was colocalized (E). HCN2-IR colocalizes with VAChT-IR, a presynaptic marker (A), (C), (D). HCN2-IR clusters that did not colocalize with VAChT-IR, colocalized with VGlut1, also a presynaptic marker (A), (B), (D), (E). Kv2.1 is a postsynaptic marker and colocalization is not present with respect to HCN2-IR (*data not shown*). Furthermore, HCN2-IR colocalizes with synaptophysin-IR, a marker for all presynaptic contacts (*data not shown*).

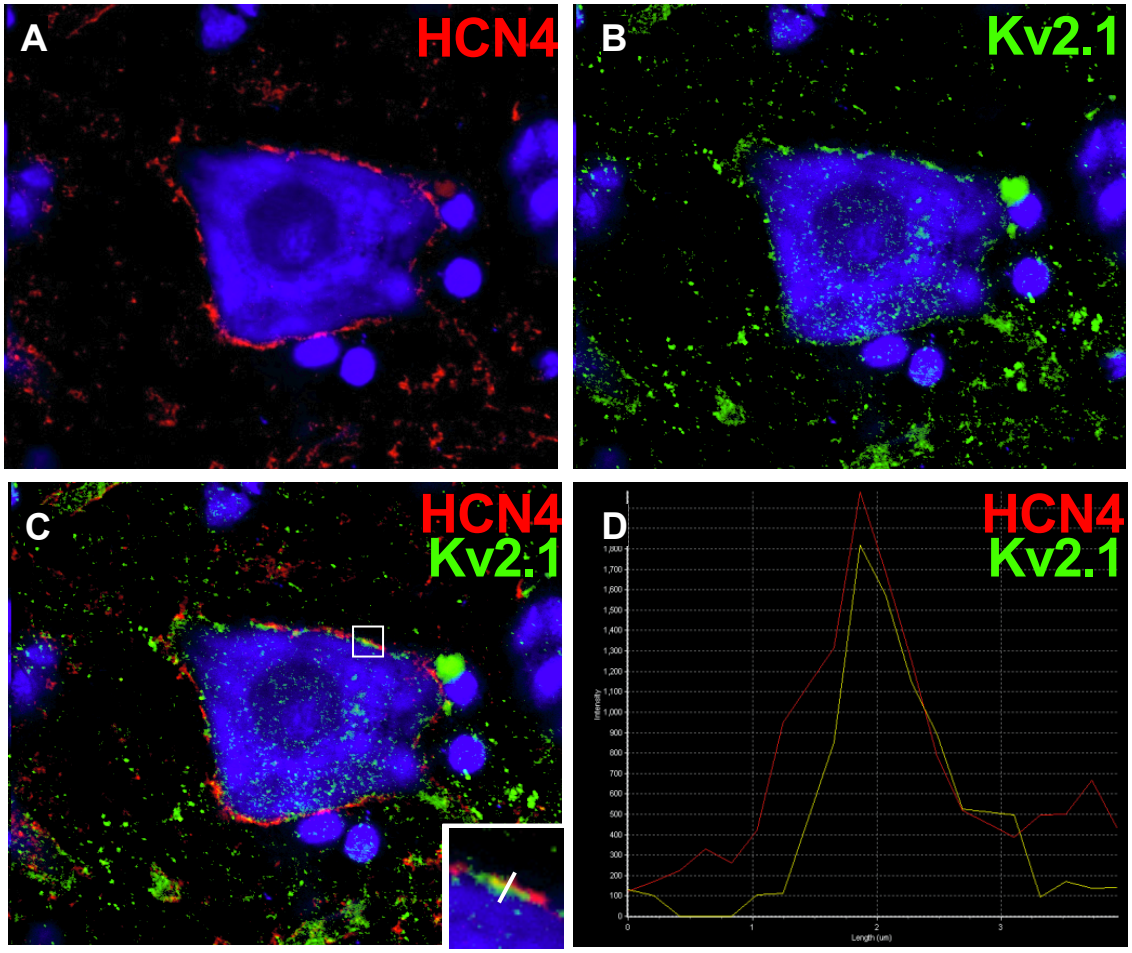
A
HCN4
B
Kv2.1
C
HCN4
Kv2.1
D
HCN4
Kv2.1
Intensity
Length (um)

Figure 4. HCN4 colocalizes with Kv2.1 demonstrating expression within the membrane. IR demonstrated that HCN4 (*red line on chart)* (D) is colocalizes with Kv2.1 (*yellow line on chart*) (D), a postsynaptic marker. However, our labeling was not consistent among all α-MNs. In some sections labeling was not precise and robust as other established antibodies.

Aim 2:

Developmental expression of HCN immunoreactivity

MNs display dramatic reorganization of intrinsic properties during development. However the developmental expression pattern of HCN isoforms and how they may underlie these changes are unknown. In various brainstem and spinal MNs, the SAG currents are either absent or greatly reduced in neonates and increase in amplitude during development (see review Carrascal, Nieto-Gonzalez, Cameron, Torres, & Nunez-Abades, 2005). This aim sought to determine the developmental expression of the various HCN isoforms to (a) determine which isoforms may be developmentally expressed, and (b) to determine if a developmental increase in HCN IR occurs at the onset of adult like locomotion (p14). One rat was euthanized, perfused, and fixed at each postnatal age of 10d, 12d, 14d, 17d, 21d, and 28d. Immunohistochemistry was then used to label for HCN1, HCN2, and HCN4. All isoforms tested had robust IR at and after p14 of age. Furthermore, there did not appear to be any alternate expression patterns of the HCN isoforms in lamina IX of the spinal cord during development. While a greater sample is needed to develop a positive correlation, the development of HCN immunoreactivity in MNs is consistent with the development of sag current. Preliminary whole cell patch clamping studies in our lab also show the absence of a robust sag current in postnatal ages younger than p14 (Patrick Sonner *pers comm*.). These developmental results help confirm that the HCN immunoreactivity is consistent with I_h current developments and further validate the antibody specificity.

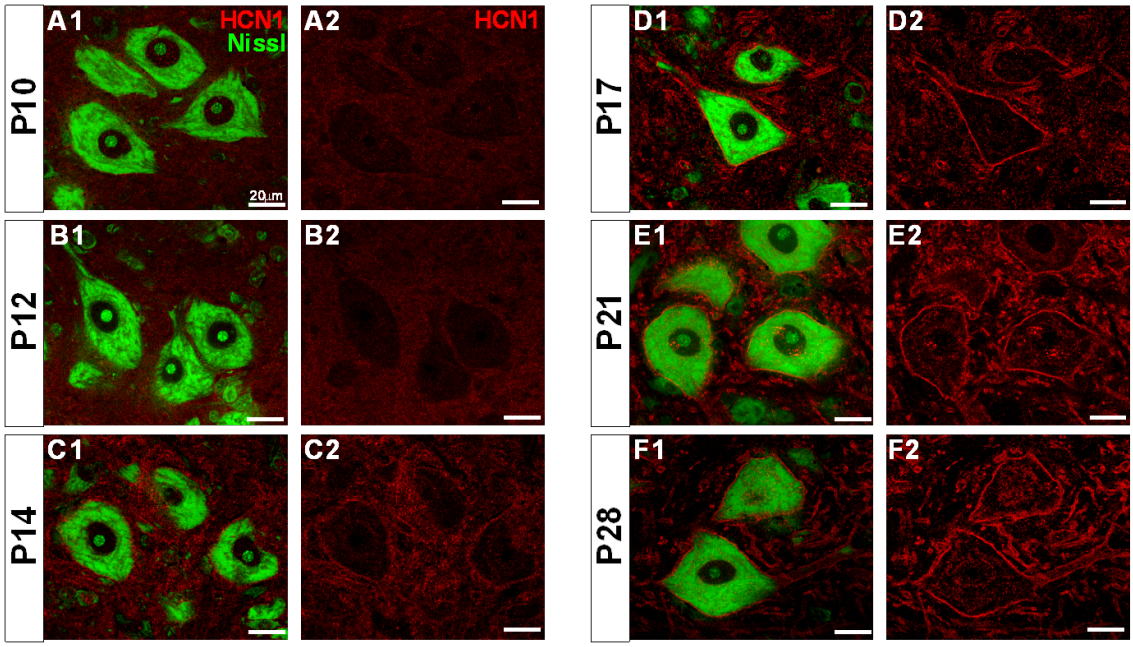
P10
A1
HCN1
Nissl
20 μm
A2
HCN1
P12
B1
B2
P14
C1
C2
P17
D1
D2
P21
E1
E2
P28
F1
F2

Figure 5. Lumbar α-motoneurons express HCN1-IR at the postnatal age of 14 days and older. HCN1-IR is robustly expressed in the MN membrane at the postnatal age of 14 days and continues to exhibit IR at future time points.

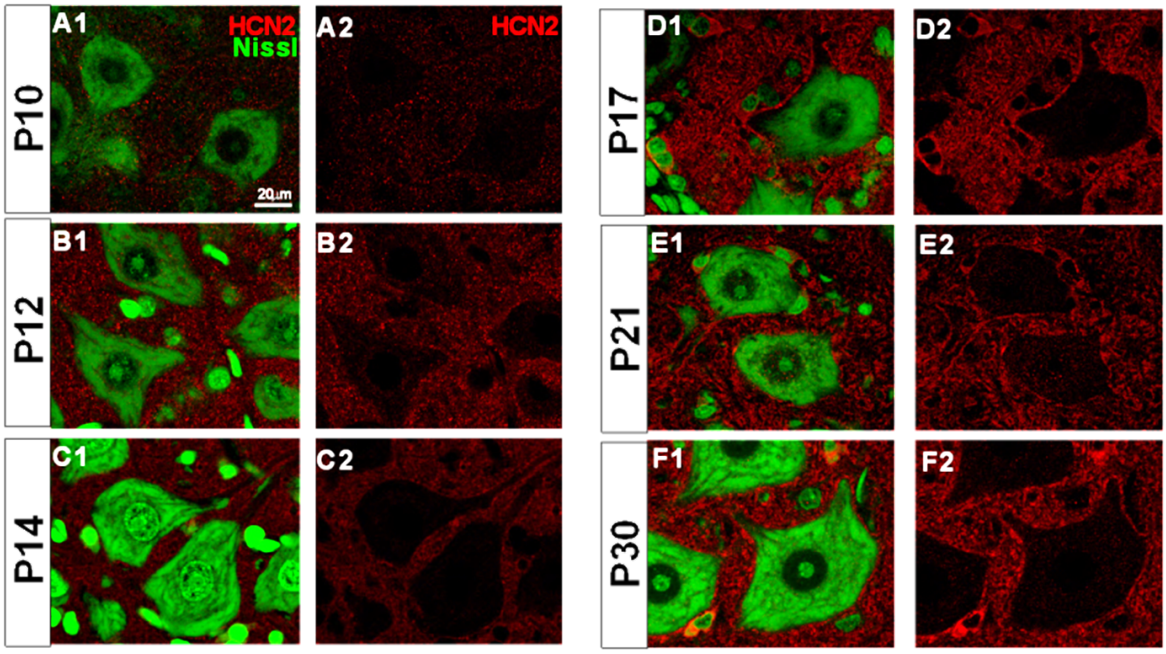
P10
A1
HCN2
Nissl
20μm
A2
HCN2
P17
D1
D2
P12
B1
B2
P21
E1
E2
P14
C1
C2
P30
F1
F2

Figure 6. Lumbar α-motoneurons express HCN2-IR at the postnatal age of 14 days and older. HCN2-IR is expressed presynaptic to the membrane at the postnatal age of 14 days and continues to exhibit this expression at future time points.

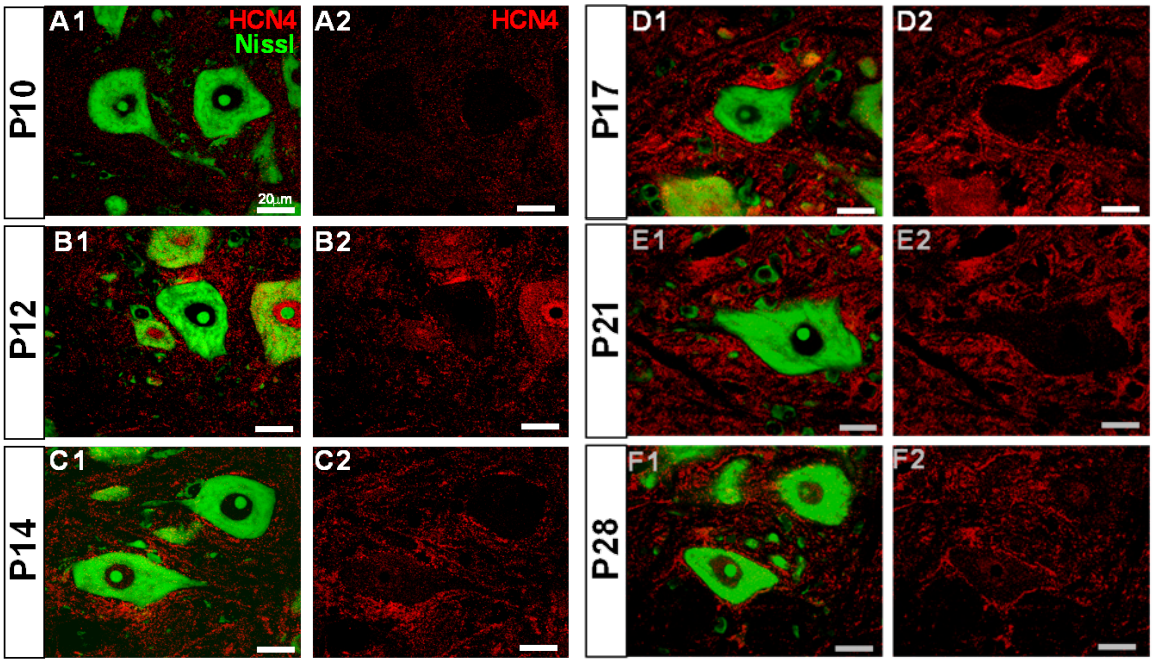
P10
A1
HCN4
Nissl
20μm
A2
HCN4
P17
D1
D2
P12
B1
B2
P21
E1
E2
P14
C1
C2
P28
F1
F2

Figure 7. Lumbar α-motoneurons express HCN4-IR at the postnatal age of 14 days and older. HCN4-IR is developmentally expressed within the membrane at the postnatal age of 14 days and continues to exhibit this expression at future time points.

Aim 3:

HCN1 Immunoreactivity in S-type vs. F-Type α-motoneurons

It has been demonstrated that the amplitude of sag current and the duration of AHP are different among MNS innervating slow-twitch muscle fibers and fast-twitch fibers. That is, MNs innervating slow-twitch muscle fibers have longer durations of AHP correlated with larger sag current amplitude when compared to MNs innervating fast-twitch muscle fibers. Because HCN channels underlie sag current, we hypothesized that S-type MN will have a lower amount of HCN1-IR when compared to F-type MN.

Retrograde tracers identified lumbar MNs with different conjugated fluorophores injected in either the predominately fast twitch Medial and lateral gastrocnemius (MG/LG) or predominately slow twitch Soleus muscle (Figure 7 A,B). MN pools containing MNs exhibiting each tracer were used for analysis. In some MN pools, MNs contained both tracers. These MNs were excluded from analysis. The MN intensity was determined by a trace of the MN somatic membrane in a single optical section. This value was normalized by diving it by the neuropil background of the optical section containing the MN of interest. The neuropil background value was created by averaging the intensity of 4 equal-sized areas of neuropil that did not contain a neuronal soma. Ten total S-Type and F-Type MNs were sampled. Neuronal area was compared between both F-type and S-type to confirm that the majority of soleus MNs were smaller in size, a characteristic of S-type MNs. The mean of F-type MN membrane traces divided by neuropil background was 3.18 with a standard error 0.33. The mean of S-type MN membrane traces divided by neuropil background was 2.22 with a standard error 0.15. The neuronal area of S-type MN were ~21% smaller than F-Type MN and displayed

~31% less intensity compared to F-Type MN (Figure 7C). Statistical significance for intensity was determined using a t-test with $p<0.05$. This experiment confirmed that S-type MN have less HCN1-IR than F-type MN.

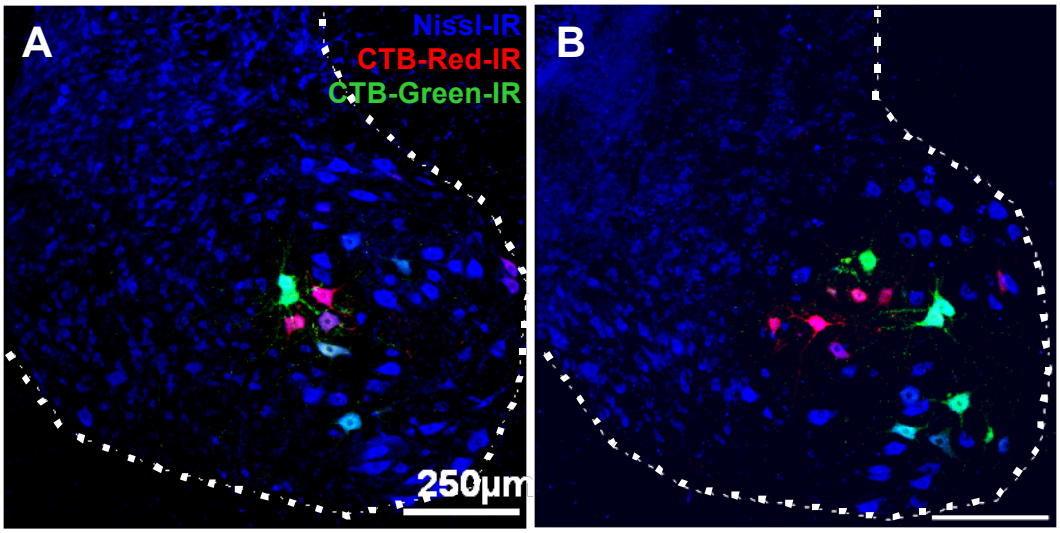
A
Nissl-IR
CTB-Red-IR
CTB-Green-IR
250µm
B

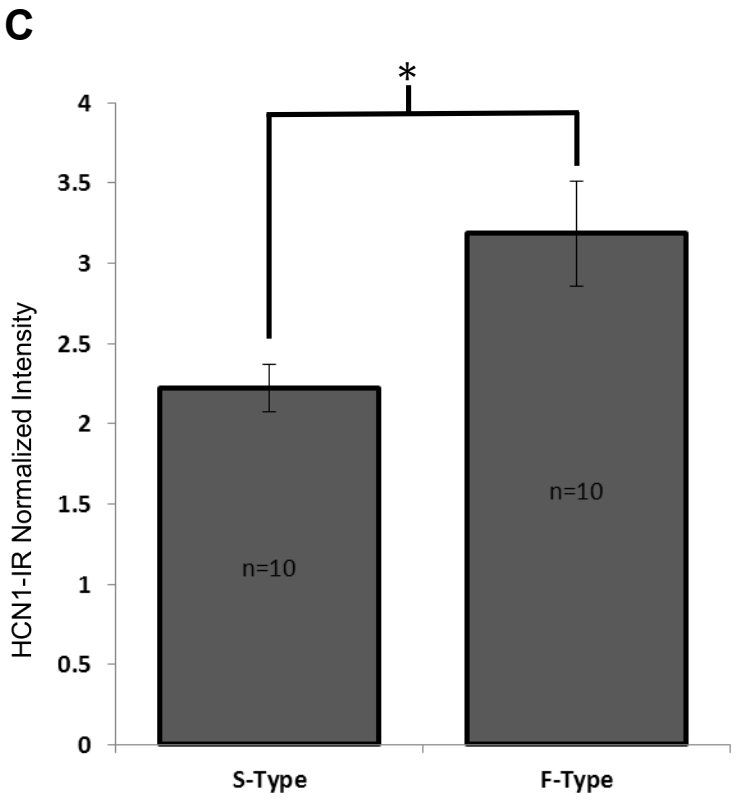
C
*
HCN1-IR Normalized Intensity
4
3.5
3
2.5
2
1.5
1
0.5
0
n=10
n=10
S-Type
F-Type

Figure 8. S-type motoneurons exhibit less HCN-IR than F-type motoneurons. S-type lumbar MNs innervating the slow twitch soleus muscle are identified with CTB-red and F-type lumbar MNs innervating the fast twitch gastrocnemius muscle are identified with CTB-red (A,B).

Aim 4:

Determine the effect of axotomy on HCN1 immunoreactivity in the soma and proximal dendrites of lumbar α-motoneurons

Peripheral nerve axotomy has been shown to affect the AHP and firing rate of α-MNs. Specifically, it was shown that a decrease in sag current amplitude was correlated with an increase in AHP duration. As HCN channels underlie sag current, this thesis attempts to correlate via IR, a decrease in expression of HCN1 channels, as a contributing factor to a decrease in sag current and increase in AHP duration α-MNs.

This aim sought to determine the expression of HCN1 channels via HCN-IR following two types of axotomy, a crush model (allows reinnervation) and a ligate model (prevents reinnervation). HCN1-IR was measured in two ways. First, the intensity of the entire MN pool was selected in confocal stacks. Second, individual MNs were selected and measured in single optical sections.

Using Fluoview software, HCN1-IR intensity was measured of the MN pool containing the injured (CTb positive) MNs (Figure 8). HCN1-IR intensity of the bilateral, uninjured MN pool of the same spinal cord histological section was also measured. Percent changes of the intensity were calculated by dividing the HCN1-IR intensity of the injured side by the HCN1-IR of the uninjured side. These values were compared to those obtained from sham experiments using a t-test with $p<0.05$. For the MN pool. significant decreases in HCN1-IR to that of control was found in the 1-day, 3-day, 8-day, and 3-month time points after the ligate injury (Figure 9). Significant

decreases were also found in the 1-day and 8-day time points of the crush injury (Figure 9).

For the somatic membrane, line traces were used to outline the membrane and measure the intensity (Figure 10). MNs exhibiting CTB were used for analysis and compared to MNs in the bilateral, uninjured MN pool of the same spinal cord histological section. Percent changes and statistical significance were determined as described above. MN traces in the cut and ligate model exhibited a sustained decrease in HCN1-IR. In the crush model, a significant decrease was observed at the 3-day and 8-day time points (Figure 11). After the 8-Day time point, HCN1-IR recovered and was closer to control (Figure 11). Results from the MN traces failed to reject our hypothesis that HCN1-IR would decrease after peripheral axotomy.

Nissl-IR was sufficient in order to observe the proximal dendrites. HCN1-IR was measured via a trace along the membrane of the dendrite in the crush injury model, starting from where the dendrite branched off of the soma. The intensity of the trace was measured in confocal stacks (8-12) of 1.0 μm steps. The length of the trace was determined by how far the HCN1-IR was observed along the dendrite. In some samples, dendritic traces were as long as 150 μm. However, sufficient data could only be obtained from trace lengths of 50 μm. A similar pattern was expressed with 3-day and 8-day time points exhibiting the greatest decrease in HCN1-IR (Figure 12). Sufficient data from sham experiments was not obtained and statistical significance of HCN-IR in proximal dendrites was not determined.

Changes in the uninjured side of the spinal cord histological section were also analyzed to determine if axotomy was producing a contralateral effect. This was

determined by dividing uninjured MN pool HCN1-IR intensities by averages of background neuropil that did not contain a MN (*as described in aim 3*) (Figure 14). No difference was observed between sham experiments and injury time points suggesting that the changes in HCN1 intensity are specific to injury and not some other effect such as glial activation or alterations in neuronal networks.

These data not only show that HCN1-IR decreases after injury but that reinnervation is necessary for its recovery. Reinnervation of the nerve occurs ~1-month after injury. Additionally, electrophysiology of the rat lumbar α-MN demonstrates that sag ratio is significantly decreased one week following a crush injury (Figure 15). The sag ratio is closer to control 1-month following injury. This observation is consistent with our HCN1-IR data (Figure 15).

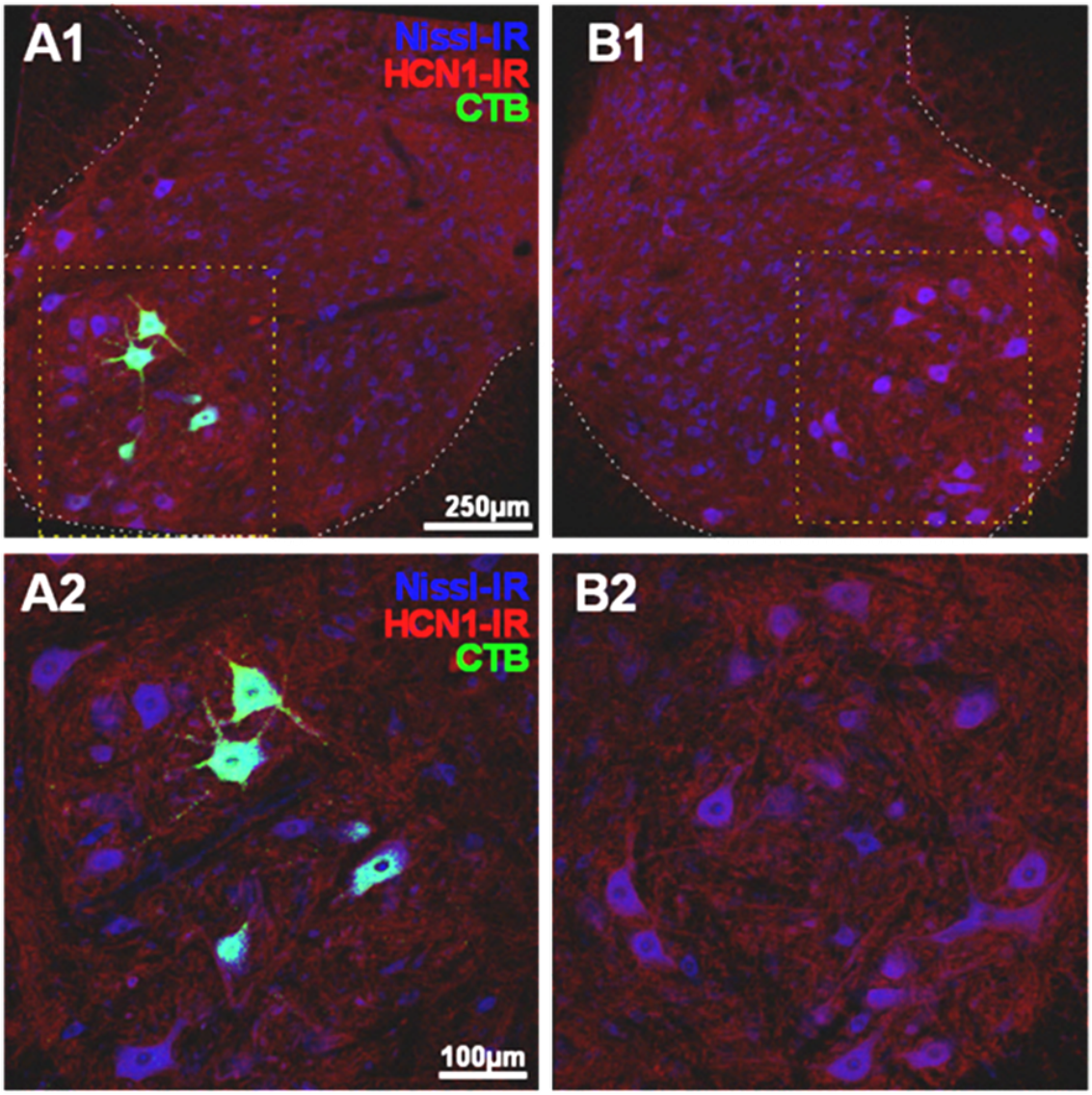
A1
Nissl-IR
HCN1-IR
CTB
250μm
B1
A2
Nissl-IR
HCN1-IR
CTB
100μm
B2

Figure 9. HCN1 immunoreactivity analysis of the motoneuron pool. Rats had either a tibial verve crush or ligate on one side leaving the other side uninjured. CTB (green) was used to label motoneurons innervating the medial and lateral gastrocnemius on the injured side of the rodent. (A1) Panels are representative of 8-12 confocal stacks at 1.0 μm steps (of HCN1-IR in red, Nissl-IR in blue as a general neuronal label. The left panel shows several MG/LG MNs on the injured side while the right panel is the bilateral uninjured side, indicated by lack of CTB-Green in the same tissue slice. A2. The average intensity of a fixed region of interest selected to include the injured MN pools, as indicated by rectangular box, was measured for both the injured and bilateral control side.

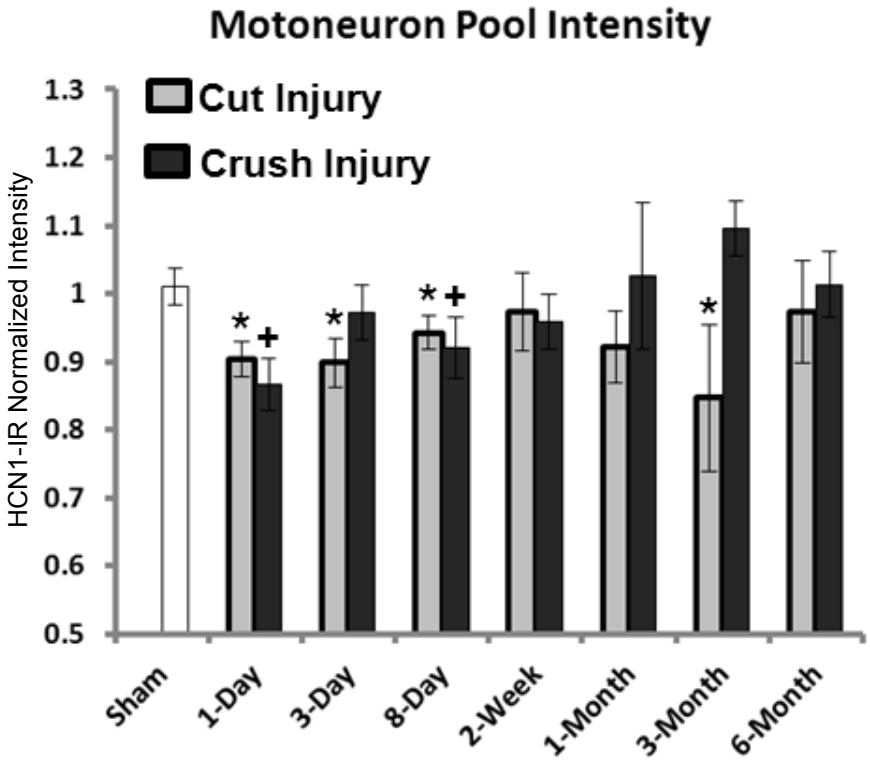
Motoneuron Pool Intensity
Cut Injury
Crush Injury
HCN1-IR Normalized Intensity
1.3
1.2
1.1
1
0.9
0.8
0.7
0.6
0.5
*
+
*
*
+
*
Sham
1-Day
3-Day
8-Day
2-Week
1-Month
3-Month
6-Month

Figure 10. HCN1 immunoreactivity of rodent lumbar motoneuron pools in the tibial nerve crush and ligate injury models returns to normal regardless of reinnervation. MN pools were measured for HCN1-IR intensity in both the tibial nerve crush model, in which reinnervation was permitted, and tibial nerve ligate model, in which reinnervation was prevented. In the ligate injury model, a statistically significant decrease in HCN1-IR was found at the 1-day, 3-day, 8-day, and 3-month time points. In the crush model, a statistically significant decrease was found at the 1-day and 8-day time points. Ten to fifteen MN pools were analyzed at each time point. Statistical significance is noted with "*" for the ligate model and "+" for crush model.

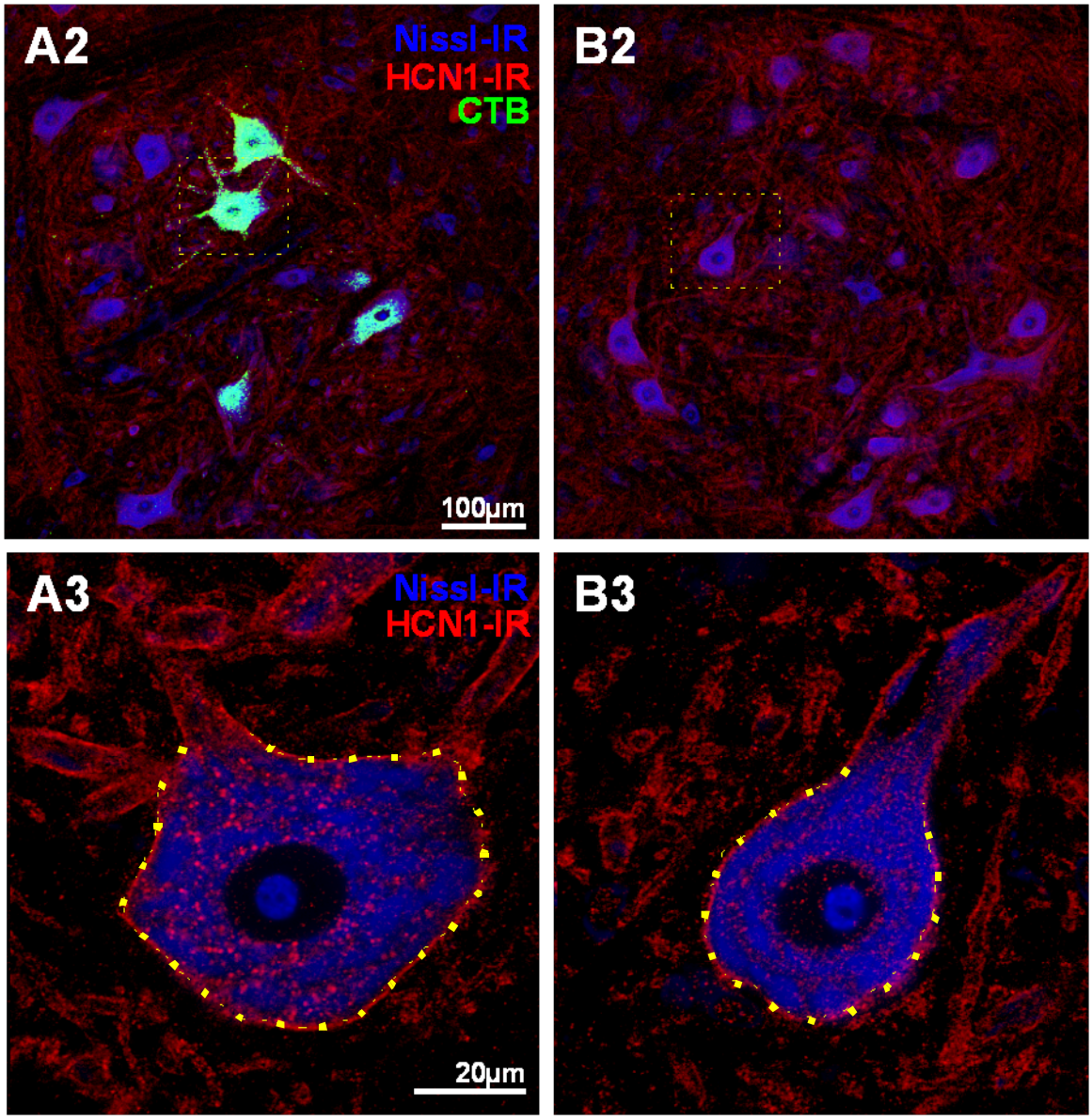
A2
Nissl-IR
HCN1-IR
CTB
100μm
B2
A3
Nissl-IR
HCN1-IR
20μm
B3

Figure 11. HCN1 immunoreactivity analysis of individual α-motoneuron. Rats had either a tibial nerve crush or ligate on one side leaving the other side uninjured. CTB (green) was used to label motoneurons innervating the medial and lateral gastrocnemius on the injured side of the rodent. (A1) Panels are representative of a single confocal section at 1.0 μm step of HCN1-IR in red, Nissl-IR in blue as a general neuronal label. The left panel shows an MG/LG MN on the injured side while the right panel is the bilateral uninjured side, indicated by lack of CTB-Green in the same tissue slice. A2. The average intensity of a MN trace selected from the injured MN pool, as indicated by the yellow dotted line, was measured for both the injured and bilateral control side. Statistical significance is noted with "*" for the ligate model and "+" for crush model.

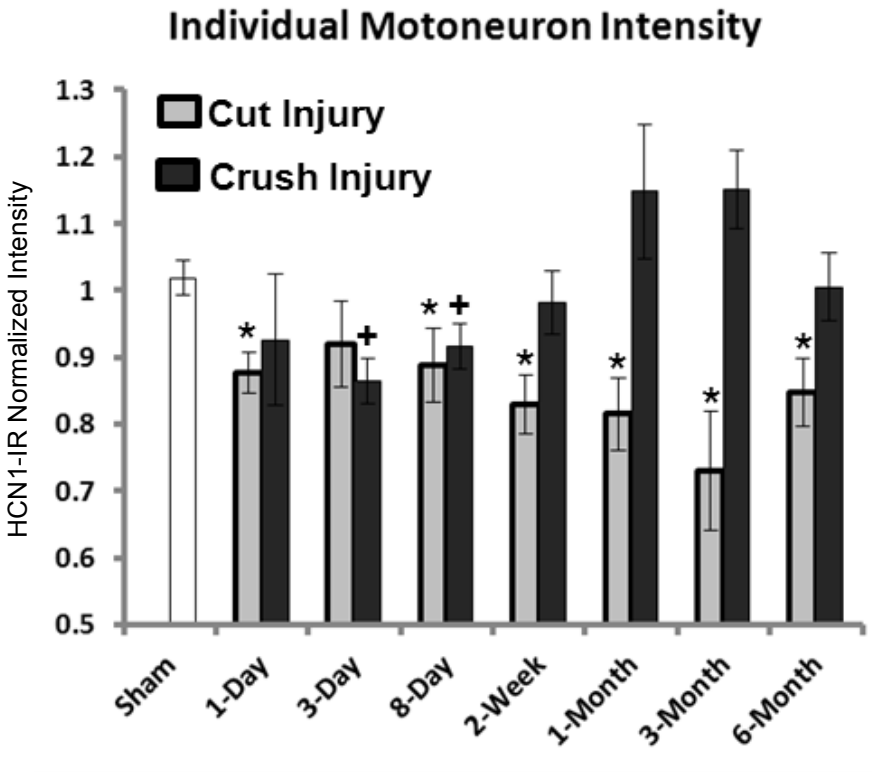
Individual Motoneuron Intensity
Cut Injury
Crush Injury
HCN1-IR Normalized Intensity
1.3
1.2
1.1
1
0.9
0.8
0.7
0.6
0.5
Sham
1-Day
3-Day
8-Day
2-Week
1-Month
3-Month
6-Month

Figure 12. HCN1 immunoreactivity of individual rodent lumbar α-motoneuron decreases with injury and requires reinnervation to return to normal. In the ligate injury model, a sustained decrease in HCN1-IR intensity was observed. A statistical significant decrease in HCN1-IR was observed in the 1-day, 8-day, 2-week, 1-month, 3-month, and 6-month time points. In the crush model, there was a statistically significant decrease at the 3-day and 8-day time points. Additionally, a higher intensity of HCN1 was observed in the crush model at the 1-month and 3-month time points, however this difference was not statistically significant.

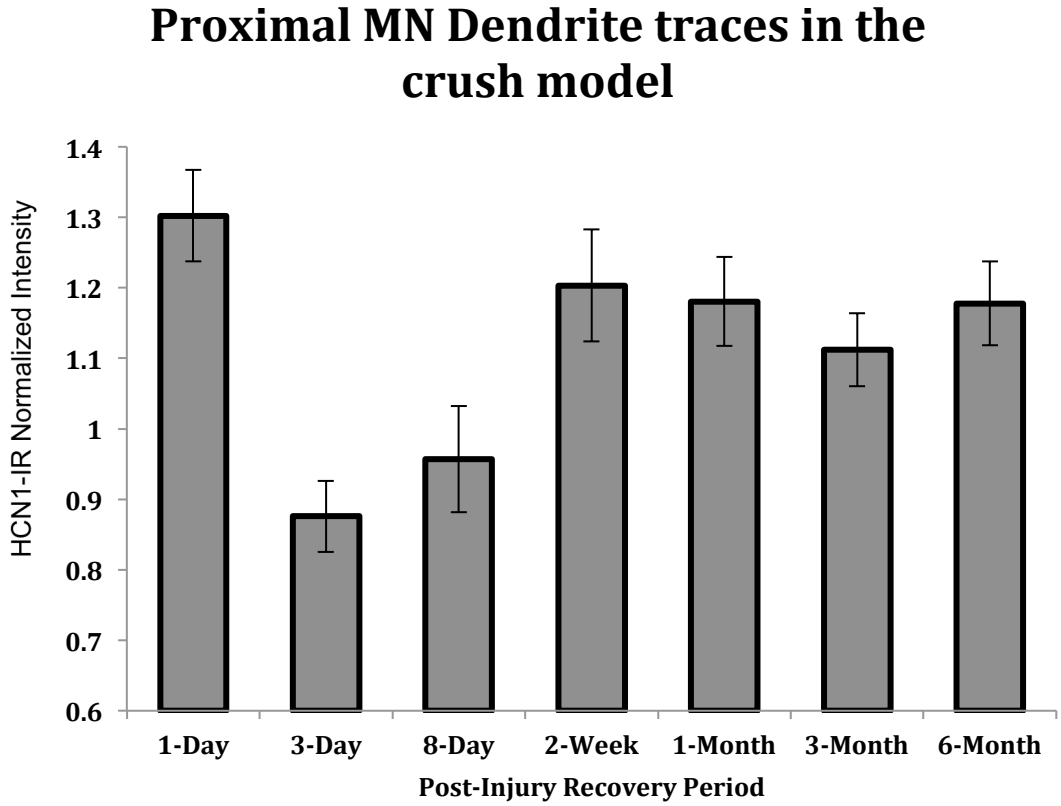
Proximal MN Dendrite traces in the crush model
HCN1-IR Normalized Intensity
1.4
1.3
1.2
1.1
1
0.9
0.8
0.7
0.6
1-Day
3-Day
8-Day
2-Week
1-Month
3-Month
6-Month
Post-Injury Recovery Period

Figure 13. HCN1-IR in the proximal dendrites of rodent α-MNs decreases following peripheral crush injury and exhibits reinnervation-dependent recovery. Dendritic traces were performed starting at the soma and continuing 50 μm distally. Intensity values from the proximal dendrite were normalized in the same fashion as previously described.

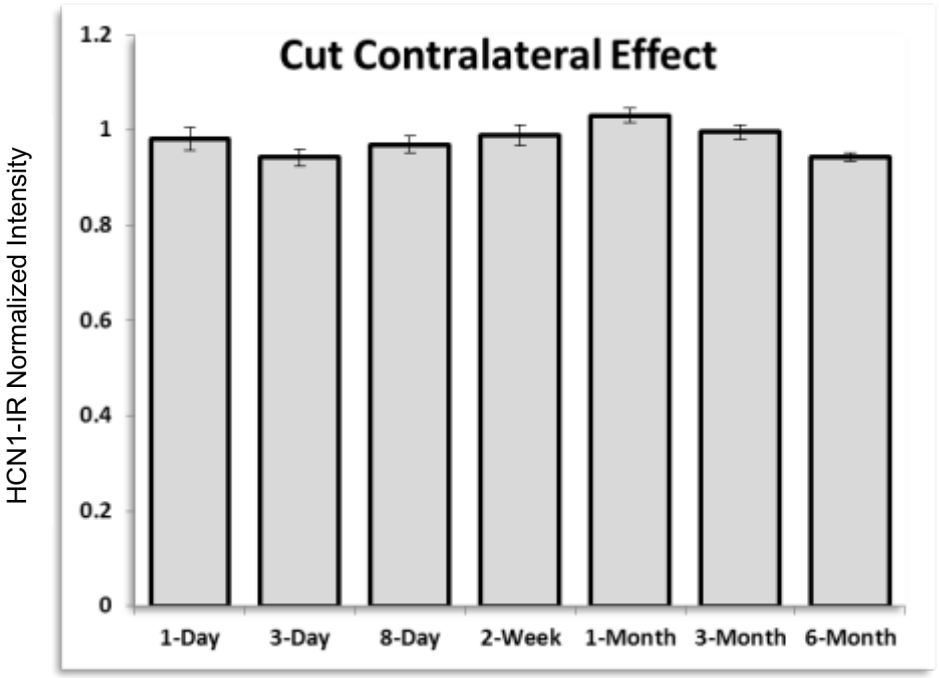
Cut Contralateral Effect
HCN1-IR Normalized Intensity
1.2
1
0.8
0.6
0.4
0.2
0
1-Day
3-Day
8-Day
2-Week
1-Month
3-Month
6-Month

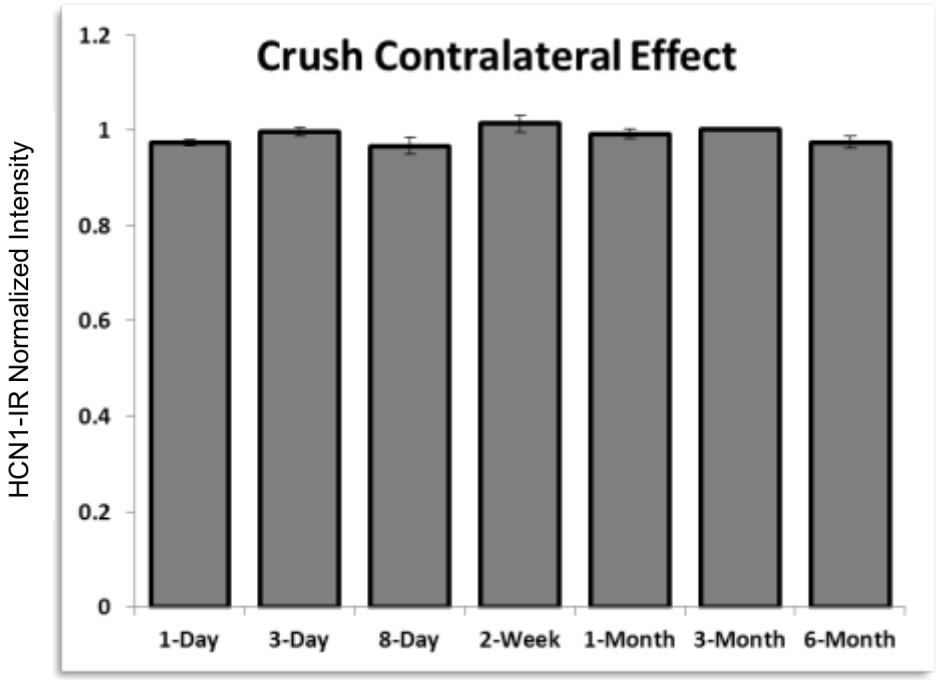
Crush Contralateral Effect
HCN1-IR Normalized Intensity
1.2
1
0.8
0.6
0.4
0.2
0
1-Day
3-Day
8-Day
2-Week
1-Month
3-Month
6-Month

Figure 14. Peripheral axotomy does not cause significant differences in HCN1-IR to the uninjured motoneuron pools. HCN1-IR on the uninjured bilateral section of the spinal cord was analyzed in order to determine the presence of a contralateral effect. In both crush model and cut and ligate model there was no significant difference in HCN1-IR for the uninjured MN pools.

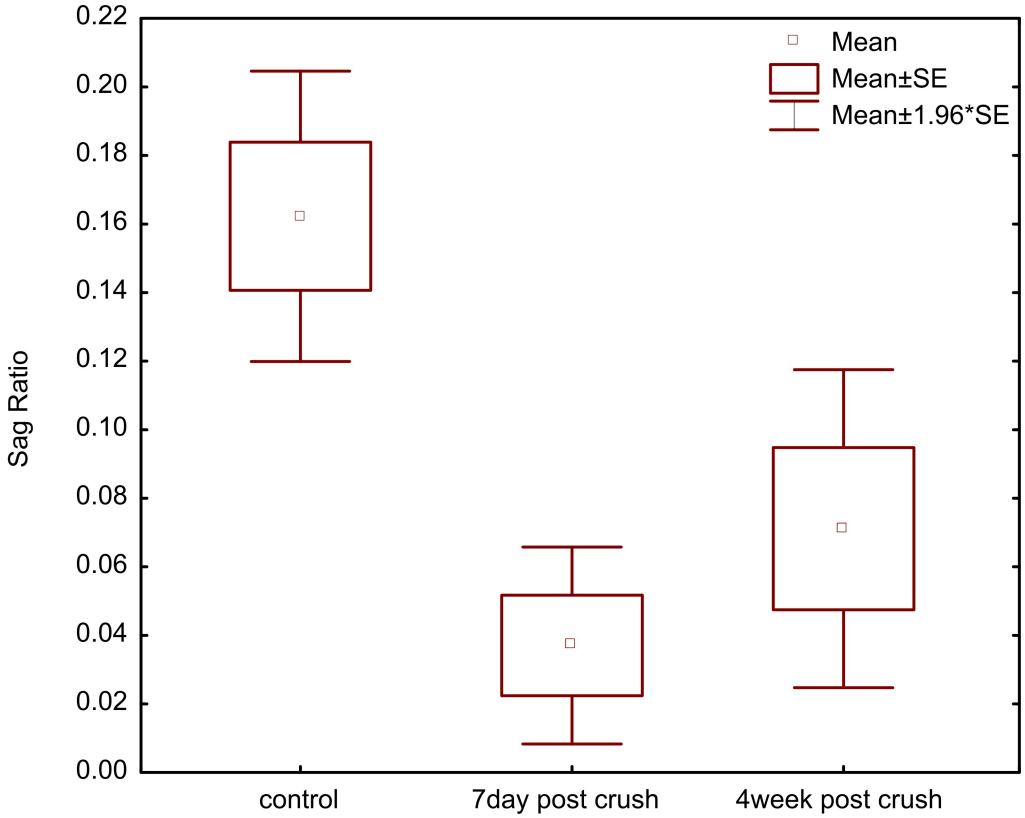
Mean
Mean±SE
Mean±1.96*SE
Sag Ratio
0.22
0.20
0.18
0.16
0.14
0.12
0.10
0.08
0.06
0.04
0.02
0.00
control
7day post crush
4week post crush

Figure 15. Sag ratio in rodent α-MNs is significantly decreased 7-days after peripheral nerve crush injury and is closer to control 4-weeks after crush injury. Sag ratio is significantly decreased 7 days after peripheral axotomy of the tibial nerve in the crush model (Adam Deardorff *pers comm*). Sag ratio values are closer to control 4 weeks after peripheral crush injury. Sag ratio was calculated by dividing the difference between the peak and the steady state potential by the difference between the peak and the baseline potential.

Conclusion

Our analysis has shown that HCN1, a known ion channel that underlies sag current, decreases in immunoreactivity in α-MN after peripheral axotomy, as indicated in our crush and ligate injury models. With reinnervation, as allowed in our crush injury model, HCN1-IR is recovered to levels exhibited in control.

VI. Discussion

A. Expression of HCN isoforms

HCN1 expression has been well characterized in the spinal cord (Milligan et al., 2006). HCN1's unique properties underlie I_h current, also known as sag. Our immunolabeling confirmed that our antibody was specifically labeling HCN1 channels located in the membrane and proximal dendrites of MNs. A western blot was used to confirm the specificity of the HCN1 antibody. The expression of HCN2 and HCN4 in spinal MNs has not yet been reported. The specificity of HCN2 and HCN4 antibodies was tested using peptide blocks. HCN1, HCN2, and HCN4 antibodies were tested in heart tissue where their expression has been established in order to confirm immunoreactivity of the epitope. Here, we have shown that HCN2 is expressed presynaptic to the membrane and is not directly related to sag current in spinal MN. Additionally, we show that HCN2 expression is colocalized at VAChT and VGlut1 synapses. HCN channels have been shown to have a critical role in synaptic transmission. Electrophysiological recordings have demonstrated the presence of I_h in several presynaptic terminals including the crustacean neuromuscular junction, avian ciliary ganglion, cerebellar basket cells, and the calyx of held in the auditory brain stem (Beaumont & Zucker, 2000; Beaumont, Zhong, Froemke, Ball, & Zucker, 2002). It was suggested that these presynaptic HCN channels play an important role in controlling synaptic transmission. In support of this hypothesis, long-term facilitation of synaptic

transmission in crustacean motor terminals was shown to be conferred by cAMP-dependent upregulation of I_h(Beaumont et al., 2002). There is initial evidence that HCN channels may directly interact with the release machinery, perhaps mediated by the cytoskeleton (Beaumont et al., 2002). Here, we have shown that HCN2, an isoform whose kinetics are affected by cAMP, is expressed presynaptically. However, in vertebrates, the functional relevance of I_h in regulating synaptic transmission is currently disputed (Chevaleyre & Castillo, 2002; Mellor, Nicoll, & Schmitz, 2002).

HCN4 immunolabeling was not as precise and robust as the HCN1 and HCN2 labeling. A colocalization study with Kv2.1 confirmed that this HCN4 was located within the membrane and could potentially contribute to sag current. It is important to note that although HCN4 was expressed within the membrane, the expression pattern is different in comparison to HCN1. For example, HCN4 is not ubiquitously expressed throughout the membrane as HCN1 is and is also present around glial cell bodies, where HCN1 is not. This provides evidence that heteromeric co-assembly is not occurring between the HCN isoforms. It also provides for the possibility of the HCN4 isoform being expressed on different MN unit types. For the purposes of this study, we focused our analysis on HCN1, but the contribution of HCN4 to post axotomy changes will be evaluated in the future.

B. Developmental Expression

This experiment provided insight into the possible changes in HCN isoform expression i.e. different isoforms being expressed at different stages developmentally. HCN1, HCN2 , and HCN4 were developmentally expressed around the p14 age.

Interestingly, at the postnatal age of 14 is when the rat begins adult like locomotion (Altman & Sudarshan, 1975). This observation provides evidence that the IR observed in our experiments are consistent with previously reported contribution of I_h to CPG (central pattern generators) networks (Kiehn et al., 2000). This experiment also provides another possible correlation between HCN1 and sag current in the α-MNs. Although multiple MNs were analyzed, only one rat was used for each time point. Thus, there may be variability in the exact age where HCN-IR begins between animals. A larger sample size and intensity analysis could be used to establish the exact time course of HCN-IR. For this thesis, this study only determined if different isoforms were being expressed developmentally and when that expression is observed.

C. F-Type vs. S-Type

S-type MN have been shown to exhibit a longer AHP and smaller sag current when compared to F-type MN (Gustafsson & Pinter, 1985). Hence, we tested to see if S-type MN had less HCN1-IR than F-type MN. Our results indicate that S-type MN had ~31% less HCN1-IR when compared to F-type MN. This distinction in properties between S-type and F-type MNs leads to further question of the response of different types of α-MNs to peripheral axotomy. Previous studies have shown that although AHP is prolonged in F-type MN after peripheral axotomy, the AHP of S-type MN is shortened (Gustafsson & Pinter, 1984a; Kuno, Miyata, & Muñoz-Martinez, 1974a; 1974b). A follow up study testing HCN1-IR in S-type MN by retrogradely labeling soleus muscle MN could determine if an increase in HCN1 expression and an increase in sag amplitude causes this AHP shortening.

D. HCN1 After Injury

As previously mentioned, this thesis attempts to characterize intrinsic changes to α-MNs after peripheral nerve injury. These intrinsic changes include a decrease in sag current correlated with an increase in AHP duration, which ultimately affects the firing rate. In this experiment we determine if HCN1-IR is altered after peripheral axotomy, and if reinnervation affects this expression. Our first analysis involved analyzing the MN pool for changes in HCN-IR after injury. Here, HCN1-IR intensity was decreased in both models at the time points of 8-day and earlier. HCN1-IR returned to normal in both models, suggesting that reinnervation was not necessary for a recovery of HCN1 expression. However, the MN pool contained both S-type and F-type MNs. As mentioned previously, studies that had shown a decrease in sag current after axotomy of F-type MN also had shown an increase in sag current for S-type MNs. This suggests that the HCN1-IR of S-type MNs may be increasing. Thus, although injured, CTB-positive MNs may be exhibiting less HCN1-IR, S-type MN in the MN pool may be exhibiting more HCN1-IR. Hence, MN pool intensities may not adequately reflect the effect of peripheral axotomy on F-type α-MNs.

After recording and analyzing the individual MN traces, a sustained decrease was observed in the ligate model. A significant decrease was also found at the 3-day and 8-day time points in the crush model. Electrophysiology recordings in the same crush injury model demonstrated a statistically significant decrease in sag ratio at 7 days post injury. The sag ratio was closer to control 1-month after injury. This finding reiterates the correlation between HCN1 and sag in the α-MN and may be the intrinsic reason that

sag is decreased and AHP duration prolonged after injury. Also shown, is the importance of reinnervation to recovery of HCN1 intensity. When reinnervation is prevented in the ligate model, a sustained decrease in HCN1-IR is observed as opposed to a recovery in HCN1-IR when reinnervation is allowed in the crush model. The crush model also provides insight into HCN1-IR with the time course of recovery of the initial injury (1day), the beginning of wallerian degeneration (3-day), the beginning of reinnervation (2week), followed by greater reinnervation (1-month and beyond). In MN pools, somatic membrane, and proximal dendrites, there was significant variability at the 1-day time points in both injury models. This variability is most likely due to the early, dynamic response after injury including the release of inflammatory cytokines and neurotrophic factors.

Although this thesis focused on the influence of HCN channel expression on sag current, another MN property that may be affected is EPSP amplitude and MN recruitability via input resistance. It has been observed that after peripheral nerve injury, EPSP amplitude increases at the 3-day time point and is below control at the 4-week time point. Our data show that HCN1-IR is lowest at the 3-day time point and above control at the 1-month time point. Also observed, in the proximal dendrites, were normalized intensity values greater than 1.0 after the 1-month time point. A decrease in HCN1-IR in the soma and proximal dendrites may be attributable to a higher input resistance and greater EPSP amplitude seen within a few days after injury, while an increase may be attributable to the opposite observation seen at the 4-week time point. Changes in input resistance would also affect changes in MN recruitment seen after injury.

In this thesis, we have attempted to analyze one of the underlying factors affecting AHP duration, firing rate, and conduction velocity after injury. Analyzing the IR of HCN channels on the MNs allowed us to determine if a change in expression of HCN channels was ultimately affecting sag current and AHP duration. It is important to note that peripheral axotomy does not cause a permanent effect on the expression of HCN1 and thus may not be a source for the absence of full motor control recovery. Our model allowed for the successful reinnervation, which is not always observed clinically. In terms of channel expression, the contribution to AHP duration from HCN1 channels in the somatic MN membrane is restored after successful regeneration and reinnervation of the nerve. Hence, clinically, in order to recover HCN1 channel expression, the use of surgical intervention and pharmacological agents are not necessary except to promote the successful regeneration and reinnervation of the nerve.

Future Studies

As previously mentioned, S-type MN have longer AHP durations and smaller sag current amplitudes when compared to F-type MN. After axotomy, the AHP of F-type MNs has been shown to increase and the AHP of S-type MNs has been shown to decrease. Here, we have shown that HCN1-IR is lesser in S-type MNs when compared to F-type MNs potentially a contributing factor to the smaller sag current and longer AHP duration. We have also shown that HCN1-IR decreases in F-type MNs after axotomy, consistent with the decrease in sag current and prolonging of AHP duration. Finally, the discrepancy between individual MN traces and MN pool intensity analysis suggests that S-type MNs may be exhibiting an increase in HCN1-IR, consistent with a previously observed increase in sag current and shortening of AHP duration. Future experiments will determine the effect of axotomy on S-type MNs. We hypothesize that HCN1-IR will increase in S-type MNs after axotomy.

References:

Altman, J., & Sudarshan, K. (1975). Postnatal development of locomotion in the laboratory rat. *Animal behaviour*, *23*, 896–920.

Altomare, C., Terragni, B., Brioschi, C., Milanesi, R., Pagliuca, C., Viscomi, C., Moroni, A., et al. (2003). Heteromeric HCN1–HCN4 Channels: A Comparison with Native Pacemaker Channels from the Rabbit Sinoatrial Node. *The Journal of Physiology*.

Alvarez, F. J., Titus-Mitchell, H. E., Bullinger, K. L., Kraszpulski, M., Nardelli, P., & Cope, T. C. (2011). Permanent central synaptic disconnection of proprioceptors after nerve injury and regeneration. I. Loss of VGLUT1/IA synapses on motoneurons. *Journal of Neurophysiology*, *106*(5), 2450–2470. doi:10.1152/jn.01095.2010

Bal, T., & McCormick, D. A. (1997). Synchronized Oscillations in the Inferior Olive Are Controlled by the Hyperpolarization-Activated Cation Current I(h). *Journal of Neurophysiology*, *77*(6), 3145–3156.

Baruscotti, M., Bottelli, G., Milanesi, R., DiFrancesco, J. C., & DiFrancesco, D. (2010). HCN-Related Channelopathies. *Pflugers Arch - European Journal of Physiology*, *460*(2), 405–415. doi:10.1007/s00424-010-0810-8

Baruscotti, M., Bucchi, A., & DiFrancesco, D. (2005). Physiology and pharmacology of the cardiac pacemaker ("funny") current. *Pharmacology & Therapeutics*, *107*(1), 59–79. doi:10.1016/j.pharmthera.2005.01.005

Beaumont, V., & Zucker, R. S. (2000). Enhancement of synaptic transmission by cyclic AMP modulation of presynaptic Ih channels. *Nature Neuroscience*, *3*(2), 133–141. doi:10.1038/72072

Beaumont, V., Zhong, N., Froemke, R. C., Ball, R. W., & Zucker, R. S. (2002). Temporal

Synaptic Tagging by Ih Activation and Actin. *Neuron*, *33*(4), 601–613. doi:10.1016/S0896-6273(02)00581-0

Bellocchio, E. E., Reimer, R. J., Fremeau, R. T. J., & Edwards, R. H. (2000). Uptake of Glutamate into Synaptic Vesicles by an Inorganic Phosphate Transporter. *Science Signaling*, *289*(5481), 957. doi:10.1126/science.289.5481.957

Bichler, E. K., Carrasco, D. I., Rich, M. M., Cope, T. C., & Pinter, M. J. (2007a). Rat motoneuron properties recover following reinnervation in the absence of muscle activity and evoked acetylcholine release. *The Journal of Physiology*, *585*(1), 47–56. doi:10.1113/jphysiol.2007.135541

Bichler, E. K., Nakanishi, S., Wang, Q.-B., Pinter, M., Rich, M., & Cope, T. (2007b). Enhanced Transmission at a Spinal Synapse Triggered In Vivo by an Injury Signal Independent of Altered Synaptic Activity. *Journal of Neuroscience*.

Biel, M., Wahl-Schott, C., Michalakis, S., & Zong, X. (2009). Hyperpolarization-activated cation channels: from genes to function. *Physiological reviews*, *89*(3), 847–885. doi:10.1152/physrev.00029.2008

Blinzinger, K., & Kreutzberg, G. (1968). Displacement of Synaptic Terminals From Regenerating Motoneurons by Microglial Cell. *Cell and Tissue Research*.

Brewster, A. L., Bernard, J. A., Gall, C. M., & Baram, T. Z. (2005). Formation of heteromeric hyperpolarization-activated cyclic nucleotide-gated (HCN) channels in the hippocampus is regulated by developmental seizures. *Neurobiology of Disease*, *19*(1-2), 200–207. doi:10.1016/j.nbd.2004.12.015

Brown, A. G., & Fyffe, R. E. (1981). Direct observations on the contacts made between Ia afferent fibres and alpha-motoneurones in the cat's lumbosacral spinal cord. *The*

Journal of Physiology, *313*, 121–140.

Brown, H., & DiFrancesco, D. (1980). Voltage-clamp investigations of membrane currents underlying pace-maker activity in rabbit sino-atrial node. *The Journal of Physiology*.

Bullinger, K. L., Nardelli, P., Pinter, M. J., Alvarez, F. J., Titus-Mitchell, H. E., & Cope, T. C. (2011). Permanent Central Synaptic Disconnection of

Proprioceptors After Nerve Injury and Regeneration. II. Loss of Functional Connectivity with Motoneurons

. *Journal of Neurophysiology*, *106*(5), 2450–2470. doi:10.1152/jn.01095.2010

Burke, R. (1967). Motor unit types of cat triceps surae muscle. *The Journal of Physiology*.

Burnett, M. G., & Zager, E. L. (2004). Pathophysiology of peripheral nerve injury: a brief review. *Neurosurgical FOCUS*, *16*(5), E1–E1.

Carrascal, L., Nieto-Gonzalez, J., Cameron, W., Torres, B., & Nunez-Abades, P. A. (2005). Changes during the postnatal development in physiological and anatomical characteristics of rat motoneurons studied in vitro. *Brain Research*.

Chan, C. S. (2004). HCN2 and HCN1 Channels Govern the Regularity of Autonomous Pacemaking and Synaptic Resetting in Globus Pallidus Neurons. *Journal of Neuroscience*, *24*(44), 9921–9932. doi:10.1523/JNEUROSCI.2162-04.2004

Chan, C. S., Glajch, K. E., Gertler, T. S., Guzman, J. N., Mercer, J. N., Lewis, A. S., Goldberg, A. B., et al. (2010). HCN channelopathy in external globus pallidus neurons in models of Parkinson's disease. *Nature Publishing Group*, *14*(1), 85–92. doi:10.1038/nn.2692

Chan, Y. M., Wu, W., Yip, H. K., & So, K.-F. (2002). Development of the regenerative capacity of postnatal axotomized rat spinal motoneurons. *Neuroreport*, *13*(8), 1071.

Chaplan, S., Guo, H., Lee, D., & Luo, L. (2003). Neuronal Hyperpolarization-Activated Pacemaker Channels Drive Neuropathic Pain. *The Journal of …*.

Chen, D. (1978). Qualitative and quantitative study of synaptic displacement in chromatolyzed spinal motoneurons of the cat. *The Journal of Comparative Neurology*.

Chen, X. Y., & Wolpaw, J. R. (1994). Triceps surae motoneuron morphology in the rat: A quantitative light microscopic study. *The Journal of Comparative Neurology*.

Chevaleyre, V., & Castillo, P. E. (2002). Assessing the role of Ih channels in synaptic transmission and mossy fiber LTP. *Proceedings of the National Academy of Sciences of the United States of America*, *99*(14), 9538–9543. doi:10.1073/pnas.142213199

Cope, T. C., Bonasera, S., & Nichols, T. (1994). Reinnervated muscles fail to produce stretch reflexes. *Journal of Neurophysiology*.

Dai, C.-F., Kanoh, N., Li, K.-Y., & Wang, Z.-M. (2000). Study on Facial Motoneuronal Death After Proximal or Distal Facial Nerve Transection. *Otology & Neurotology*, *21*(1), 115.

DiFrancesco, D. (1986). Characterization of single pacemaker channels in cardiac sino-atrial node cells. *Nature*, *324*(6096), 470–473. doi:10.1038/324470a0

Doan, T. (1999). Contribution of the hyperpolarization-activated current to the resting membrane potential of rat nodose sensory neurons. *The Journal of Physiology*.

Dum, R. P., O'Donovan, M. J., Toop, J., Tsairis, P., Pinter, M. J., & Burke, R. E. (1985). Cross-reinnervated motor units in cat muscle. II. Soleus muscle reinnervated by

flexor digitorum longus motoneurons.

Eccles, J., Eccles, R., & Lundberg, A. (1958). The action potentials of the alpha motoneurones supplying fast and slow muscles. *The Journal of Physiology*, *142*(2), 275–291.

Eser, F., Aktekin, L., Bodur, H., & Atan, C. (2009). Etiological factors of traumatic peripheral nerve injuries. *Neurology India*, *57*(4), 434. doi:10.4103/0028-3886.55614

Fenrich, K., & Gordon, T. (2004). Axonal regeneration in the peripheral and central nervous systems--current issues and advances. *The Canadian journal of neurological sciences. Le journal canadien des sciences neurologiques*, *31*(2), 142–156.

Foehring, R., & Sypert, G. (1986). Properties of self-reinnervated motor units of medial gastrocnemius of cat. II. Axotomized motoneurons and time course of recovery. *Journal of ….*

Foehring, R., Sypert, G., & Munson, J. (1986). Properties of self-reinnervated motor units of medial gastrocnemius of cat. I. Long-term reinnervation. *Journal of Neurophysiology*.

Fugleholm, K., & Schmalbruch, H. (1994). Early peripheral nerve regeneration after crushing, sectioning, and freeze studied by implanted electrodes in the cat. *The Journal of ….*

Fyffe, R. E. (2001). *Spinal motoneurons: Synaptic inputs and receptor organization*. (T. C. Cope, Ed.) (pp. 21–46). Motor neurobiology of the spinal cord.

George, M. S., Abbott, L. F., & Siegelbaum, S. A. (2009). HCN hyperpolarization-activated cation channels inhibit EPSPs by interactions with M-type K+ channels. *Nature Neuroscience*, *12*(5), 577–584. doi:10.1038/nn.2307

Gorassini, M., Bennett, D., & Kiehn, O. (1999). Activation Patterns of Hindlimb Motor Units in the Awake Rat and Their Relation to Motoneuron Intrinsic Properties. *Journal of ….*

Gossen, E. R. (2003). The time course of the motoneurone afterhyperpolarization is related to motor unit twitch speed in human skeletal muscle. *The Journal of Physiology*, *552*(2), 657–664. doi:10.1113/jphysiol.2003.048132

Granit, R., Phillips, C., Skoglund, S., & Steg, G. (1957). Differentiation of tonic from phasic alpha ventral horn cells by stretch, pinna and crossed extensor reflexes. *Journal of Neurophysiology*, *20*(5), 470–481.

Gustafsson, B., & Pinter, M. J. (1984a). Effects of axotomy on the distribution of passive electrical properties of cat motoneurones. *The Journal of Physiology*, *356*, 433–442.

Gustafsson, B., & Pinter, M. J. (1984b). Relations among passive electrical properties of lumbar a-motoneurones of the cat. *The Journal of Physiology*, *356*, 401–431.

Gustafsson, B., & Pinter, M. J. (1985). Factors determining the variation of the afterhyperpolarization duration in cat lumbar α-motoneurons. *Brain Research*, *326*(2), 392–395. doi:10.1016/0006-8993(85)90053-8

Haftel, V. K., Bichler, E. K., Wang, Q.-B., Prather, J. F., Pinter, M. J., & Cope, T. C. (2005). Central suppression of regenerated proprioceptive afferents. *Journal of Neuroscience*, *25*(19), 4733–4742. doi:10.1523/JNEUROSCI.4895-04.2005

Havton, L., & Kellerth, J. (1990). Elimination of Intramedullary Axon Collaterals of Cat Spinal U-Motoneurons Following Peripheral Nerve Injury *Experimental brain research*.

Kandel, E. R., Schwartz, J. H., & Jessell, T. M. (1991). *Principles of neural science* (p.

1135).

Kellerth, J., & Brannstrom, T. (1998). Changes in Synaptology of Adult Cat Spinal -Motoneurons After Axotomy. *Experimental brain research*.

Kiehn, O., Kjaerulff, O., Tresch, M. C., & Harris-Warrick, R. M. (2000). Contributions of intrinsic motor neuron properties to the production of rhythmic motor output in the mammalian spinal cord. *Brain research bulletin*, *53*(5), 649–659.

Kuno, M., Miyata, Y., & Muñoz-Martinez, E. J. (1974a). Differential reaction of fast and slow alpha-motoneurones to axotomy. *The Journal of Physiology*, *240*(3), 725–739.

Kuno, M., Miyata, Y., & Muñoz-Martinez, E. J. (1974b). Properties of fast and slow alpha motoneurones following motor reinnervation. *The Journal of Physiology*, *242*(1), 273–288.

la Cruz, De, R., & Pastor, A. (1994). Effects of Target Depletion on Adult Mammalian Central Neurons: Morphological Correlates. *Neuroscience*.

Leao, K. E., Leao, R. N., Sun, H., Fyffe, R. E. W., & Walmsley, B. (2006a). Hyperpolarization-activated currents are differentially expressed in mice brainstem auditory nuclei. *The Journal of Physiology*, *576*(3), 849–864. doi:10.1113/jphysiol.2006.114702

Leao, R. N., Sun, H., Svahn, K., Berntson, A., Youssoufian, M., Paolini, A. G., Fyffe, R. E. W., et al. (2006b). Topographic organization in the auditory brainstem of juvenile mice is disrupted in congenital deafness. *The Journal of Physiology*, *571*(3), 563–578. doi:10.1113/jphysiol.2005.098780

Lee, S. K., & Wolfe, S. W. (2000). Peripheral Nerve Injury and Repair. *Journal of the American Academy of Orthopaedic Surgeons*, *8*(4), 243–253.

Ludwig, A., Budde, T., Stieber, J., Moosmang, S., Wahl, C., Holthoff, K., Langebartels, A., et al. (2003). Absence epilepsy and sinus dysrhythmia in mice lacking the pacemaker channel HCN2. *The EMBO Journal*, *22*(2), 216–224. doi:10.1093/emboj/cdg032

Ludwig, A., Zong, X., Stieber, J., Hullin, R., Hofmann, F., & Biel, M. (1999). Two pacemaker channels from human heart with profoundly different activation kinetics. *The EMBO Journal*, *18*(9), 2323–2329. doi:10.1093/emboj/18.9.2323

Lüscher, H. R., & Clamann, H. P. (1992). Relation between structure and function in information transfer in spinal monosynaptic reflex. *Physiological reviews*, *72*(1), 71–99.

Lüthi, A., & McCormick, D. A. (1998). H-current: properties of a neuronal and network pacemaker. *Neuron*, *21*(1), 9–12.

Maccaferri, G. (1996). The hyperpolarization-activated current (Ih) and its contribution to pacemaker activity in rat CA1 hippocampal stratum oriens-alveus interneurones. *The Journal of Physiology*.

MacDermid, V. E., Neuber-Hess, M. S., & Rose, P. K. (2003). The temporal sequence of morphological and molecular changes in axotomized feline motoneurons leading to the formation of axons from the ends of dendrites. *The Journal of Comparative Neurology*, *468*(2), 233–250. doi:10.1002/cne.10966

Madison, R. D., Archibald, S. J., & Brushart, T. M. (1996). Reinnervation accuracy of the rat femoral nerve by motor and sensory neurons. *The Journal of neuroscience : the official journal of the Society for Neuroscience*, *16*(18), 5698–5703.

Magee, J. (2000). Dendritic integration of excitatory synaptic input. *Nature Reviews*

Neuroscience.

Mellor, J., Nicoll, R. A., & Schmitz, D. (2002). Mediation of hippocampal mossy fiber long-term potentiation by presynaptic Ih channels. *Science (New York, N.Y.)*, *295*(5552), 143–147. doi:10.1126/science.1064285

Milligan, C. J., Edwards, I. J., & Deuchars, J. (2006). HCN1 ion channel immunoreactivity in spinal cord and medulla oblongata. *Brain Research*, *1081*(1), 79–91.

Miyata, Y., & Yasuda, H. (1988). Enhancement of Ia synaptic transmission following muscle nerve section: dependence upon protein synthesis. *Neuroscience research*, *5*(4), 338–346.

Molander, C., Xu, Q., & Grant, G. (1984). The cytoarchitectonic organization of the spinal cord in the rat. I. The lower thoracic and lumbosacral cord. *The Journal of Comparative Neurology*, *230*(1), 133–141. doi:10.1002/cne.902300112

Moosmang, S., Stieber, J., Zong, X., Biel, M., Hoffman, F., & Ludwig, A. (2001). Cellular expression and functional characterization of four hyperpolarization-activated pacemaker channels in cardiac and neuronal tissues. *European Journal …*.

Nakanishi, S., Cope, T., Rich, M., Carrasco, D., & Pinter, M. J. (2005). Regulation of Motoneuron Excitability via Motor Endplate Acetylcholine Receptor Activation. *Journal of Neuroscience*.

Noma, A., & Irisawa, H. (1976). Membrane currents in the rabbit sinoatrial node cell as studied by the double microelectrode method. *Pflugers Archiv European Journal of Physiology*, *364*(1), 45–52. doi:10.1007/BF01062910

Notomi, T., & Shigemoto, R. (2004). Immunohistochemical localization of Ih channel

subunits, HCN1–4, in the rat brain. *The Journal of Comparative Neurology*, *471*(3), 241–276.

Pape, H. (1996). Queer current and pacemaker: the hyperpolarization-activated cation current in neurons. *Annual review of physiology*.

Pape, H.-C., & McCormick, D. A. (1989). Noradrenaline and serotonin selectively modulate thalamic burst firing by enhancing a hyperpolarization-activated cation current. *Nature*, *340*(6236), 715–718. doi:10.1038/340715a0

Pian, P., Bucchi, A., Robinson, R. B., & Siegelbaum, S. A. (2006). Regulation of gating and rundown of HCN hyperpolarization-activated channels by exogenous and endogenous PIP2. *The Journal of general physiology*, *128*(5), 593–604. doi:10.1085/jgp.200609648

Poolos, N. P., Bullis, J. B., & Roth, M. K. (2006). Modulation of h-channels in hippocampal pyramidal neurons by p38 mitogen-activated protein kinase. *Journal of Neuroscience*, *26*(30), 7995–8003. doi:10.1523/JNEUROSCI.2069-06.2006

Richichi, C., Brewster, A. L., Bender, R. A., Simeone, T. A., Zha, Q., Yin, H. Z., Weiss, J. H., et al. (2008). Mechanisms of seizure-induced "transcriptional channelopathy" of hyperpolarization-activated cyclic nucleotide gated (HCN) channels. *Neurobiology of Disease*, *29*(2), 297–305. doi:10.1016/j.nbd.2007.09.003

Robinson, R. B., & Siegelbaum, S. A. (2003). Hyperpolarization-activated cation currents: from molecules to physiological function. *Annual review of physiology*, *65*, 453–480. doi:10.1146/annurev.physiol.65.092101.142734

Rose, P. K., & Odlozinski, M. (1998). Expansion of the dendritic tree of motoneurons innervating neck muscles of the adult cat after permanent axotomy. *The Journal of*

Comparative Neurology, *390*(3), 392–411. doi:10.1002/(SICI)1096-9861(19980119)390:3<392::AID-CNE7>3.0.CO;2-X

Santoro, B., Liu, D., Yao, H., Bartsch, D., & Kandel, E. (1998). Identification of a Gene Encoding a Hyperpolarization-Activated Pacemaker Channel of Brain. *Cell*.

Shi, W., Wymore, R., Yu, H., Wu, J., Wymore, R. T., Pan, Z., Robinson, R. B., et al. (1999). Distribution and prevalence of hyperpolarization-activated cation channel (HCN) mRNA expression in cardiac tissues. *Circulation research*, *85*(1), e1–6.

Stoll, G., & Muller, H. (1999). Nerve Injury, Axonal Degeneration and Neural Regeneration: Basic Insights. *Brain pathology*.

Stoll, G., Reiners, K., Schwendemann, G., Heininger, K., & Toyka, K. V. (1986). Normal myelination of regenerating peripheral nerve sprouts despite circulating antibodies to galactocerebroside in rabbits. *Annual Neurology*, *19*(2), 189–192. doi:10.1002/ana.410190213

Sumner, B. (1975). A Quantitative Analysis of Boutons with Different Types of Synapse in Normal and Injured Hypoglossal Nuclei. *Experimental neurology*.

Sumner, B., & Sutherland, F. I. (1973). Quantitative Electron Microscopy on the Injured Hypoglossal Nucleus in the Rat

. *Journal of neurocytology*.

Swett, J., Wikholm, R., Blanks, R., & Swett, A. (1986). ScienceDirect.com - Experimental Neurology - Motoneurons of the rat sciatic nerve. *Experimental …*.

Wainger, B. J., DeGennaro, M., Santoro, B., Siegelbaum, S. A., & Tibbs, G. R. (2001). Molecular mechanism of cAMP modulation of HCN pacemaker channels. *Nature*, *411*(6839), 805–810. doi:10.1038/35081088

Wang, J., Chen, S., & Siegelbaum, S. A. (2001). Regulation of hyperpolarization-activated HCN channel gating and cAMP modulation due to interactions of COOH terminus and core transmembrane regions. *The Journal of general physiology*, *118*(3), 237–250.

Yanagihara, K., & Irisawa, H. (1980). Inward current activated during hyperpolarization in the rabbit sinoatrial node cell. *Pflugers Archiv European Journal of Physiology*, *385*(1), 11–19. doi:10.1007/BF00583909

Yu, F. H. (2005). Overview of Molecular Relationships in the Voltage-Gated Ion Channel Superfamily. *Pharmacological Reviews*, *57*(4), 387–395. doi:10.1124/pr.57.4.13

Zolles, G., Klöcker, N., Wenzel, D., Weisser-Thomas, J., Fleischmann, B. K., Roeper, J., & Fakler, B. (2006). Pacemaking by HCN Channels Requires Interaction with Phosphoinositides. *Neuron*, *52*(6), 1027–1036. doi:10.1016/j.neuron.2006.12.005